MECHANICAL AND RHEOLOGICAL CHARACTERISATION OF 3D FIBRONECTIN-COLLAGEN FIBRILLAR SCAFFOLDS

Parisa Sadeghi

Thesis submitted to the University of Ottawa in partial Fulfillment of the requirements for Master of Science

Department of Physics
Faculty of Science
University of Ottawa

Abstract

The extracellular matrix (ECM) is a complex fibrillar network that couples a cell with its environment and directly regulates the cell's fate via structural, mechanical, and biochemical signals. The goal of this thesis was to engineer and characterize ECM-mimicking protein platforms with material properties covering both physiological and pathological tissues.

First, we fabricated three-dimensional (3D) fibrillar scaffolds comprising the two major components of the ECM, namely collagen (COL) and fibronectin (FN), using a temperature-controlled casting technique to regulate the rate of protein gelation and consequently scaffold fibres' density. Second, we assessed the material properties of the COL-FN scaffolds, in the presence (cell-laden) and absence (ECM only) of cells, to establish a correlation between their structural and mechanical characteristics. As structural scaffold characterization was the object of a previous thesis in our laboratory (in brief the higher the casting temperature, the denser the scaffolds result), the present work focused on exhaustive mechanical characterization. Here we report the quantification of both elastic and viscous properties of all scaffolds, when subjected either to compression or shear, using two different tools and protocols.

In our first approach, we used a Dynamic Mechanical Analyzer (DMA) to compress the scaffolds and record consecutive force-indentation profiles, from which we extracted overall stiffness through the slope of the converted stress-strain profiles. The scaffolds were immersed in PBS and after 24hr, were compressed up to 25% strain, at a velocity of 25 μm/s. Although our numerous experiments suggested that denser scaffolds tended to have higher Young's moduli than their sparse counterparts, the DMA technique did not allow us to establish a significant difference in stiffness between them.

In our second approach, we used a Rheometer to subject the scaffolds to oscillatory shear stresses and assess their viscoelasticity by measuring their storage modulus (G') and loss modulus (G''), characteristics of their elastic and viscous behaviours, respectively. After performing initial amplitude sweeps to determine the linear viscoelastic regime and set a desirable amplitude of deformation for further analysis (here 0.25%), various frequency sweeps were performed with strain rate ranging from 0.1 to 10 (1/s) at 0.25% amplitude of deformation. Our results clearly indicate that, in the absence of cells, dense scaffolds (composed of short and thin fibres) were

both stiffer and more viscous than sparse scaffolds (composed of long and thick fibres). Our data also show that, unexpectedly, the presence of cells significantly decreases both stiffness and viscosity of dense scaffolds, while it increases them when scaffolds are less dense. Finally, all scaffolds exhibited a dominating elastic response.

Collectively, our study shows that we were able to generate both ECM and cell-ECM scaffolds with controlled volume, density, elasticity, and viscous characteristics. These tunable platforms enable a better understanding of the critical link between ECM structure and mechanics, with the ultimate goal of controlling cellular functions. As such they represent a valuable tool for biomaterials and biophysics research, with many potential applications in basic research, medical diagnosis and tissue engineering.

Table of Contents

List of Figures

Acknowledgements

First, I would like to express my deepest gratitude to my advisor Prof. Delphine Gourdon for her essential advice and continual support. It was a great privilege and honour to work and study under the supervision of such a knowledgeable scientist. I have been influenced and inspired by her patience and encouragement.

I would like to thank Dr. James L. Harden for his guidance and help in carrying important experiments throughout this project. I also thank my thesis committee members, Dr. Xudong Cao and Dr. James L. Harden.

My special sincere gratitude goes to Ryan Hickey from Dr. Pelling's lab for training me on how to work with the micromechanical device. To my supportive and mindful friends here, Naveena Narayanan and Halimo Aden, thank you for your positive words and your intellectual support.

I am also grateful to the present member of the Gourdon lab, Javad Eslami, and past members: Maryam Asadishekari, Elie Ngandu Mpoyi, and Mihir Samak for their contributions at the time I joined the group. This work could not be finished without Fan Wan's. Thank you for accompanying me in the lab even during the tough and weird times of the pandemic.

I would like to thank my special friend Kamyar Tavakoli for his moral support. Thank you for your unwavering support at my side constantly even when the times got rough. I am also extremely grateful to his kind-hearted family for their caring and encouragement.

Last but not least, I wish to express my warmest gratitude to my caring and loving parents who have always supported me unconditionally. Any attempt at any level cannot be satisfactorily completed without their encouragement and confidence. I also would like to thank my lovely brothers and my lovely sister-in-law for their spiritual support.

List of Abbreviations

2D	Two dimensional
3D	Three dimensional
α-MEM	Minimum Essential Medium Eagle - alpha modification
AFM	Atomic Force Microscopy
ANOVA	Analysis of variance
COL	Collagen
DMA	Dynamic Mechanical Analyzer
ECM	Extracellular matrix
FBS	Fetal bovine serum
FN	Fibronectin
LVR	Linear Viscoelastic Region/Regime
PBS	Phosphate buffered saline
VEGF	Vascular endothelial growth factor

Chapter 1 – Introduction 3D ECM-Mimicking Tunable Scaffolds

1.1 Introduction

The extracellular matrix (ECM), a three-dimensional (3D) network, is the microenvironment of cells and is composed of cell-secreted molecules. It provides biochemical and structural support to most tissues, cells, and organs. Cells reside in the ECM which, in turn, generates signals that control cellular behaviour. Mechanical and chemical characteristics of the ECM determine these signals.[1] The reciprocal mechanical interaction that exists between a cell and the ECM [2] has an impact on essential cell functions linked to whole organ activities. It is well recognized that changes in ECM characteristics in particular changes in ECM composition and stiffness are involved in pathological conditions such as cancer.[3] The study of cell behaviour (e.g., migration, proliferation), as well as the mechanical characteristics of the 3D ECM-mimicking environment, will provide crucial insights into the progression of cancer. It also can provide approaches to limit progression and prevent metastatic conditions in the end. The intrinsic dependency of mechanical characteristics of the matrix on its microstructure makes it a key research interest of materials science. In fact, ECM mechanical properties are regulated through modifications of the microstructure and the composition of the matrix. This chapter introduces ECM components, cancer progression and application of biomaterials to mimic ECM structures.

1.2 Soft Tissues

Biological tissues are classified into hard tissues such as bone and teeth and soft tissues such as cartilage and skin. Minerals are the main components of hard tissues while the major component of soft tissues is interstitial water. This difference causes distinct mechanical characteristics. In contrast to mineralized tissues, soft connective tissues may be different for their high flexibility (i.e., undergo large deformations). Biological soft tissues show viscoelastic behaviour, which is a time-dependent behaviour combination of both elastic and viscous components. They usually behave anisotropically and their mechanical properties are highly sensitive to testing conditions. Mechanical properties of soft tissues subjected to load vary by age, pH, and the rate of applied load or deformation. Also, changing the degree of hydration of soft tissues can significantly alter their viscoelasticity, which is why one needs to be extremely cautious during characterization, to maintain in native/biological conditions.[4]

Finally, biological tissues display a wide range of mechanical behaviours, in particular stiffness, which spans from 100 Pa for the softest organs, like the brain or cartilage, to ten thousand Pa (MPa range) in muscle tissues, up to the GPa range in cortical bone. In soft connective tissues, the structural arrangement and the concentration of major components like collagen can also change their mechanical properties.[5]

1.3 Extracellular Matrix (ECM)

The ECM is a heterogeneous network composed of several macromolecules with specific physical and biochemical properties.[6] Although it is mostly composed of water, fibrous proteins, proteoglycans, and glycosaminoglycans (GAGs) are the main structural constituents of the ECM.[7] It also acts as a reservoir of bioactive molecules and growth factors. There are two structural forms of ECM. The basement membrane (two-dimensional (2D)) and the interstitial matrix (3D fibrillar ECM).[8] Cells are connected to the interstitial matrix by the basement membrane that is comprised of a less porous and more compact structure (sheet-like). In contrast, interstitial ECM is a hydrated scaffold forming a fibrillar matrix around cells.[9] The ECM composition varies from tissue to tissue according to their functions and to the cells they contain (which are also the cells that secreted it). For example, tendons mostly comprise collagen I while, in basement membranes, laminins and collagen IV are ubiquitous.[10] Once they deposit the ECM, cells are able to sense its signals mainly through trans-membrane proteins, called integrins, known to transduce mechanical forces into biochemical events (a.k.a. mechanotransducer proteins).

Several studies have reported that ECM physical properties control processes such as cell migration[11], spreading[12], differentiation[13] and proliferation.[14] It is also well established that, in connective tissue pathologies, alteration of mechanical [7], structural and/or morphological characteristics of ECM [15] and its chemical composition [16] can affect cellular behaviour. The structural and mechanical properties of the native ECM are intrinsically related, and modification of mechanical characteristics of the matrix usually requires some degree of changes in its structure/morphology. Changes in the microarchitecture of collagen networks have been reported to mechanically regulate many reciprocal cell-ECM interactions.[17] Composition (upregulation of one protein with respect to another) is also a key contributor to matrix alterations. For instance, it has been shown that ECM components deposition can lead to ECM stiffening, as it increases the density of the matrix. In other words, alteration in the density of ECM is associated with an

overexpression of ECM proteins mainly fibrillar collagen type I [18], which results in overall ECM stiffening.[19] Investigations on the effects of collagen accumulation on ECM characteristics demonstrated that deposition of collagen increased epithelial cell proliferation and cancer risk.[20] Additionally, Levental et al. showed that breast tumorigenesis is accompanied by collagen crosslinking and increased focal adhesions.[21]

Several studies have shown that mechanical cues from the ECM affect various cell functions in both 2D and 3D environments. It was reported that cells cultured onto stiff substrates spread widely [14][22] and migrate rapidly, while on softer substrates spreading area decreases. Stiffness of ECM regulates the structure of cultured cells: it was observed that on soft substrates (comparable to normal brain tissue) cells appear uniformly rounded and then cannot migrate efficiently.[14][22] Cell proliferation is also controlled by ECM stiffness, with cells able to divide much faster onto stiffer ECMs.[14] Additionally, differentiation of stem cells in particular mesenchymal stem cells (MSCs) is increased on stiff matrices.[23][24] However, it later appeared that elasticity alone did not reflect the complex mechanics of all signalling of ECM, which is a highly viscoelastic material. Therefore, many functions of cells were later shown to depend on the viscous response of the ECM. For instance, the matrix deposited by breast cancer conditioned cells exhibited not only higher stiffness but also higher viscosity (more specifically higher dissipation), which in turn affected their adhesion and growth factor signalling.[25] Specific investigations of substrate viscosity showed that increased viscosity led to increased spreading and proliferation of human MSCs while reducing the size and maturity of focal adhesions (FAs).[26] Finally, in an exhaustive study of cell interactions with purely viscous surfaces, it was shown that substrate viscosity is entirely responsible for cell morphology: with low-viscosity surfaces resulting in small and rounded cells while high-viscosity surfaces showed large and highly spread cells.[27]

Therefore, investigating the full array of ECM mechanical and structural characteristics is essential, as it will allow us to (i) understand some complicated biological functions, such as cancer progression, and (ii) design and engineer better ECM-mimicking scaffolds for cancer mechanobiology research in controlled environments.

1.3.1 Collagen

Collagen is the key structural protein of ECM. It is a long fibrous protein that shows abilities to regulate cell morphology, migration, and differentiation.[28][29] Collagen is the main protein not only of most soft tissues such as blood vessels, nerves, and skin but also harder tissues such as cartilage, ligaments, and bone.[30] The osteoblasts and the fibroblasts are the two cell types that synthesize collagen in bone, dermis, and tendons. Among 28 different types of fibrillar and non-fibrillar collagen that have been identified, fibril-forming collagens (Type I, II, III) are the most common types. Collagen type I is soluble in dilute acid and constitutes approximately 30% of the total proteins of the body's tissues. Source of collagen type I can be rat tail tendon or bovine calf skin among other sources.[31]

Collagens are macromolecules with a length of approximately 280 nm, which most prominent feature is the formation of a triple helical structure. This triple helix is formed by three collagen polypeptide α chains (specifically, two α1 chains and one α2 chain in the case of collagen type I). The primary structure of each α chain is a Gly-X-Y amino acid repeating triplet motif. High glycine content in collagen is a necessary condition for the formation of the tightly woven structure of the triple helix, which then confers rigidity to collagen fibres.[32] Triple helices are first assembled into thin collagen microfibrils that are then cross-linked to form larger collagen fibres.[33] Depending on their arrangement and their degree of crosslinking, collagen fibres confer either high stiffness as in bones, compliance as in tendons, or rigidity gradient as in cartilage. Additionally, collagen type I plays a significant role in the viscoelasticity of tissues (even in bones). Collagen fibrils' diameter can also vary greatly, which confers varied strength to tissues.

Ehrman and Gey in 1956 proposed collagen as a platform for cell culture. Biocompatibility, low toxicity besides the chemical, physical and immunological properties [34] make the collagen solution a preferable biomaterial in tissue engineering, drug delivery and wound healing. Collagen I upon changing the pH, easily forms a hydrogel.[35] It may be processed alone or in combination with other materials to create cell scaffolds for bone regeneration, nervous [36], and vascular system repair.[37]

1.3.2 Fibronectin

Fibronectin (FN) is a fibril-forming glycoprotein, which main role is to mediate cell-matrix adhesion. It is a ubiquitous protein in embryonic tissues and wound healing, and it is needed not only in most dynamic processes of tissues like growth and wound hemostasis, but also in the progression of diseases such as fibrosis and cancer.[38] FN is a large multi-modular dimeric protein, composed of two similar monomeric subunits linked by two C-terminus disulphide bonds, with an overall molecular weight varying from 460 to 540 kDa.[39] Three types of modules comprise FN, namely FN I, FN II and FN III. While FN I and FN II modules contain internal disulphide bonds, which confer them a stable folded structure, FN III modules lack disulphide bonds and are less stable, especially under mechanical forces.[40] As a consequence, some binding sites of FN, called cryptic sites, are hidden within the molecule when it is in its folded or equilibrium form and become exposed when FN is stretched [41], as described in detail below.

Considered a mechanotransducer protein, FN is able to undergo sequential changes in its structure upon strain, from compact to elongated to fully unfolded, which then dramatically affects its function.[42] When force/cell-induced protein unfolding occurs, cryptic sites may become exposed.[43] The exposure of cryptic sites controls a wide range of cell-matrix interactions, and also affects the binding/release of important growth factors.

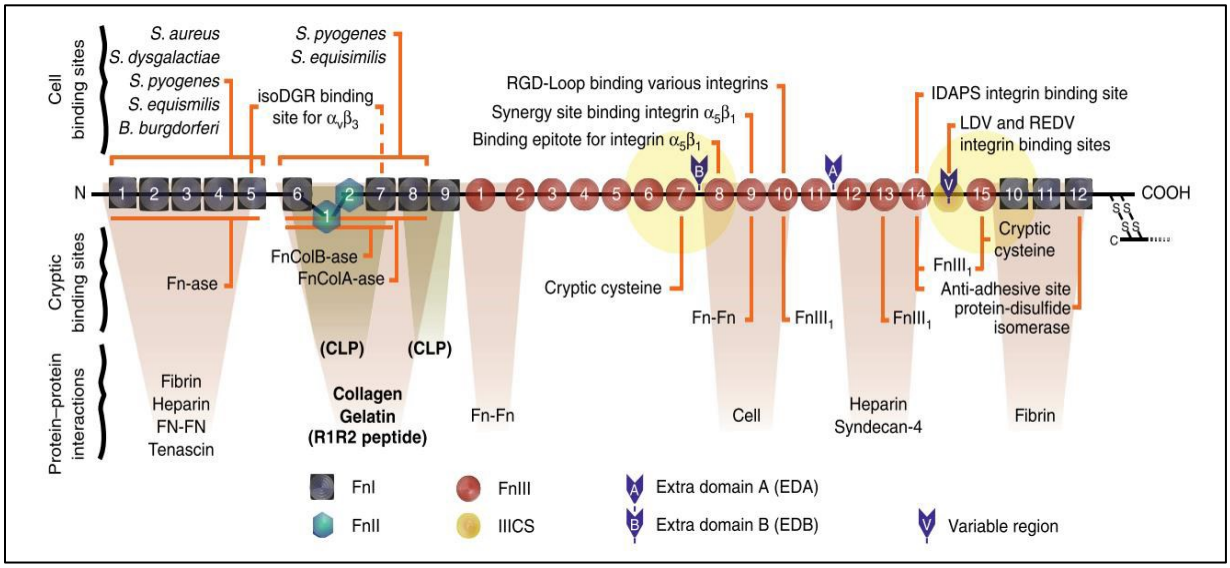

Figure 1.1 **Schematic of FN molecule (only one monomer is shown) displaying type I, II, and III modules with their associated exposed and cryptic binding sites.** Adapted from [44].

The lack of disulphide bonds in FN III modules makes them sensitive to structural changes. As shown in Figure 1.1, there are fifteen type III modules, twelve type I modules and only two type II modules on each FN monomer. FN III1 (also called anastellin) is one of the most important binding sites on FN, as it assists FN aggregation into fibrils. FN with various functions can interact and bind to cells and other molecules simultaneously because of the numerous binding sites present.[45] There are multiple recognition sites in FN for cells including the well-defined RGD loop (Arg-Gly-Asp) and other ECM proteins such as collagen (I_{6-9} and $II_{1,2}$) and fibrin (Fibrin I and Fibrin II).[46]

FN I with 45 amino acids contains a double-stranded anti-parallel β-sheets as well as a triple-stranded antiparallel β-sheets knit together. FN II comprises 40 amino acids and two perpendicular antiparallel β-sheets.[47] Because of the presence of disulphide bonds in modules I and II responsible for their stabilization, it is unlikely to see any major alteration in their conformation. On the other hand, FN III modules are larger (90 amino acids distributed in seven beta-strands arranged in two antiparallel sheets) with two important recognition sites for cells: the RGD loop which resides on III_{10} and the synergy site that is located on the adjacent FN III_9. These recognition sites make the FN III_{9-10} one of the most crucial sequences in FN since most cell-binding interactions are associated with the exposure (and integrity) of the RGD loop. Some integrins such as αvβ3 need only the RGD loop to bind to FN.[48] In contrast, other integrins such as α5β1 require an extra binding site, pro-his-ser-arg-asp (PHSRN) synergy site.[40]

There are two forms of FN: soluble inactive (plasma FN) that circulates in the blood and insoluble active form (cellular FN). The insoluble form of FN is deposited by cells, it comprises highly elastic polymerized fibrils formed by cell/integrin-mediated forces.[49] Plasma FN functions at the early stages of wound healing and hemostasis. Cellular FN is involved in the late stages of wound healing, fibrosis, and angiogenesis.[50] FN plays major functions in different applications. It enhances cell-tissue interaction in the skin and also helps to repair tissue structures through wound healing.[51] Conformation of FN is crucial in various processes, as any alteration (extension and/or partial unfolding) of its secondary and/or tertiary structure may impact the exposure or disruption of binding sites and consequent cell signalling. FN molecules bind to integrin receptors on cells that activate signalling pathways to promote cell attachment, migration, and differentiation.[52] In the compact form of FN, its arms are crossed over (pretzel shape) whereas, in the unfolded form, FN's arms are separated and some secondary structure is lost.[46]

It has been established that FN is the first ECM protein cells deposit when forming most new tissues.[53] The early FN framework then controls the deposition and assembly of collagen fibres in the cell environment.[54] In tissues, a large range of FN conformations usually coexist: for example, it was shown in a 3D tissue morphogenesis model that there are at least one compact and one extended FN populations. In the compact form, FN is adsorbed to collagen while in the extended FN, it forms an independent fibrillar network that does not colocalize with the collagen present in the tissue.[54]

1.4 Biomaterials

In tissue engineering, biomaterials refer to materials interacting with biological systems for the evaluation, treatment or replacement of tissues, organs and body functions.[55] To obtain a better understanding of biological functions, it is essential to develop efficient and reliable 3D platforms that mimic all tissue properties in their native conditions. In particular, biomaterials can be manufactured to accurately mimic the soft native ECM and control cellular behaviour.[56] Biomaterials are grouped into three classes of natural, synthetic, and hybrid materials, which are used for the fabrication of tissue engineering scaffolds. Synthetic biomaterials such as metals, ceramics, polymers, and composites are used in several applications.

Metals are used for specific biomedical applications due to their mechanical properties including high strength, fatigue endurance limit and toughness.[57] Specifically, they are used in dental and orthopedic implants, for example in bone screws, hip and knee prosthesis.[58] In addition, some metals are used as electrodes (platinum) in neural implants and various cardiovascular implants such as in heart valves and pacemakers.[59] Overall, stainless steel, cobalt, titanium and their alloys are the most commonly used metals in these applications. Ceramics' properties include inertness, high strength, wear-resistance, and durability, which make them ideal for use as coatings for both cardiovascular and orthopedic implants. The most common ceramics used in the body are alumina, zirconia, bioactive glass and hydroxyapatite.[60]

Finally, polymeric materials are extensively used in the medical field because of the wide range of properties (and processing techniques) among all the biomaterials. Polymers can be very diverse in composition and properties. They can be used both in long-term implantable devices in neurological, cardiovascular implants and in short-term applications such as wound treatment, skin replacement, and/or dental fillings. Polyvinylchloride (PVC), polyethylene (PE), and

polymethylmethacrylate (PMMA) are the most common polymers used in medical fields. Note that the basic composition of hard tissues such as bone consists of natural polymers, i.e., collagen and ceramics (hydroxyapatite), which together confer rigidity and strength. The combination of biomaterials into composite materials is a common technique to achieve better mechanical strength and resistance to fatigue since they often overcome limitations found in pure metals, ceramics, and/or polymers individually. Composites are widely used in orthopedics and cardiovascular applications as well as biosensors and microelectrodes.[60]

The difference between conventional materials and biomaterials is that biomaterials need to possess one extra key property: biocompatibility. In such a context, low biocompatibility and/or lack of interaction with the surrounding tissue of synthetic biomaterials make natural biomaterials like collagen, chitosan, fibrin, and alginate more preferable. Natural polymers are hydrophilic and generally highly biocompatible because of their similar chemical composition to biological tissues. In general, natural materials consist of proteins, polysaccharides, and polynucleotides, and they have a huge impact on human healthcare. The source of natural biomaterials are plants, animals, or humans. Biomaterials are chosen according to the type of application, the cost, and the complexity of its purification and engineering process. Natural scaffolds derived from tissues or organs, called decellularized tissues (since cells need to be removed to avoid foreign body reactions) have attracted attention due to their natural protein contents and matrix-mimicking properties. Although they have been used in cartilage sheets [61] and orthopedic scaffolds [62], the structure (and accurate composition) of decellularized tissues such as density and shape can hardly be controlled. To use natural biomaterials, donor tissues also need to be provided.[63]

1.5 Hydrogels and Fibrillar Scaffolds

In such context, hydrogels have recently gained lots of interest in biomaterials science and biomedical engineering. A hydrogel is a network made of aqueous-dispersed hydrophilic polymer chains, with a broad range of tunable physical and chemical properties. The polymeric network is assembled through several methods including physical association, ionic and chemical crosslinking.[64] Among the various hydrogel assembly methods, the gelation process is the physical association of the polymer chains that generally occurs in response to temperature variations. This alteration is the result of a temperature-induced change in the solubility of the polymer chains, which promotes the close packing of polymer backbones into rigid structures.[65]

Hydrogels composed of biological polymers (e.g. actin, collagen, and fibrin) are often used as ECM models for the study of cell-matrix interactions. [31] In the case of collagen-based scaffolds, hydrogel formation is generated by collagen gelation, which is similar to naturally occurring fibril formation called fibrillogenesis. In this case, the neutralized native acid-soluble collagen molecules (Type I) start forming a hydrogel when both temperature and pH raise to reach the physiological conditions at which the hydrophilic polymer chains naturally crosslink (self-assembly).

Over the past 50 years, the interest in hydrogels for biomedical applications, tissue engineering and drug delivery intensified due to their unique features. These properties refer to their aqueous nature, biodegradability and tissue-mimicking mechanical properties.[66] Their elasticity is able to span across several orders of magnitude depending on the structure of the polymeric network. Increasing the polymer molecular weight and crosslinker concentration can easily increase the elasticity of the gels. Such elasticity control makes them widely utilized in medicine.[67] Hence hydrogels are good mimetics of biological tissues (in the swollen state) because they display similar properties, not only mechanical (remarkable elasticity) but also chemical (high hydrophilicity). Another interesting feature of hydrogels is that they can be generated in large volumes (3D hydrogels) to better mimic realistic cellular microenvironments and study, for example, the role of matrix mechanics on various cell functions. In fact, several studies, particularly in cancer research, have revealed that 3D cell cultures (e.g., breast adenocarcinoma cells) behave considerably differently than 2D cell cultures (carried out on top of polyacrylamide gels or in standard Petri dishes), as they display large differences in cell-cell and cell-matrix interactions, as well as in cell mechanics. As the cell development process in native conditions (in vivo) is not entirely replicated by 2D (monolayer) systems, key cellular functions such as cell proliferation, differentiation, apoptosis, and migration were shown to greatly differ in 2D and 3D cell culture models.[68] Breast cancer cells cultured in 2D and 3D platforms showed significant differences in morphology and cytoskeletal organization. In particular, when MCF-7 cells (a breast cancer cell line) were seeded either onto alginate-coated dishes (2D) or within 3D alginate gels, they exhibited significant differences in morphology: flat and organized in monolayers on the 2D substrate, while round and organized in clusters (similar to those in vivo) within the 3D gels.[69] 3D cell cultures also show gene expression profiles [70] and responses to

treatment [71] more similar to in vivo state, as cells are in direct contact with their matrix in all spatial dimensions.[72]

When specifically considering mechanical properties, 3D hydrogels are also very useful to replicate ECM viscoelastic networks and investigate independently the effect of various parameters (such as elasticity and/or stress relaxation) on cell behaviour. Importantly, Chaudhuri and coworkers were the first to report that both cell spreading and proliferation were greater in 3D substrates exhibiting faster stress relaxation [12] regardless of the initial elastic modulus of hydrogels.[73] The same group later showed that osteogenic differentiation of mesenchymal stem cells (MSCs) was also enhanced in cells cultured in fast relaxing 3D hydrogels.[74]

In tissue engineering, many scientists attempt to engineer platforms that replicate the ECM. 3D collagen-based scaffolds alone or in combination with other ECM proteins is a common approach to develop better ECM-mimicking substrates in terms of biological, chemical, and mechanical properties.[75] Collagen and/or FN, which allow cells to bind to substrates, are typically used with cells using several methods of fabrication. Early on, 2D collagen platforms were obtained by simply incubating collagen onto the surface of polyacrylamide or other gels surface and using a crosslinker. As a result, cells would adhere to the gel surface coated with collagen fibres.[76] As described in detail in Section 1.3, native ECM consists of a protein network made of fibres that are deposited and assembled by cells (fibrillogenesis process). However, most engineered 3D hydrogels mentioned earlier in this Section exhibit a porous morphology rather than an actual fibrillar structural network, which differs significantly from the ECM. In fact, fibrillar scaffolds are better mimetics of the ECM and are critical for the formation of focal adhesions, that mediate cell-signalling pathways.[77] This indicates that 3D fibrillar networks enable crucial cell-matrix interactions through integrins, as well as some remodelling of the local collagen matrix needed for the development of focal adhesions.[76] More recently, engineered 3D scaffolds made of fibrillar FN have been reported to be a promising approach for cancer research, as they promoted cell invasion and proliferation, enabled in vitro expansion of primary cancer cells and induced an epithelial-to-mesenchymal transition in cancer cells.[78] As described below, the tumour microenvironment can affect cancer progression by interrupting or promoting cancer cell growth. Therefore, developing 3D platforms for large volumes and long cell culture times will provide a better understanding of tumour growth and metastasis.[79]

1.6 Cancerous Tissues

The "seed and soil" hypothesis is a key concept in cancer research. This theory indicates that, in addition to the presence of cancer cells (seed), the cells' microenvironment (soil) is also important. Healthy and tumour microenvironments have shown significant differences in structural and mechanical properties. Evidence indicates that during tumour progression and cancer metastasis, ECM is constantly modified in terms of composition, morphology (density) and stiffness.[80][81] Many studies focused on individual cells to find a relationship between their mechanical characteristics and different physiological and/or pathological conditions.[82] For instance, MCF-7 cancer cells (cultured in 3D environments) showed higher proliferation within stiffer substrates.[69]

In a normal microenvironment, ECM collagen fibres are sparse, curly, and compliant while in the neighbourhood of breast cancer cells, they are abundant and thick, aligned in parallel bundles and stiff.[83] Several studies of breast cancer, pancreatic cancer, gastric cancer, and prostate cancer revealed that the accumulation of fibrillar collagen in the stroma increases ECM density which leads to overall tissue stiffening.[84][85][86] High density and increased stiffness of the ECM were also shown to promote angiogenesis, which is directly linked with tumour growth.[80]

As mentioned earlier, because they are more compliant and lack crosslinking, FN fibres are able to respond to environmental stresses: they can be mechanically stretched by cells and can consequently extend/unfold in tissues [87], which alters their biological functions and makes them sensitive mechanotransducers.[88] It has been shown that FN deposition is upregulated in several types of cancer [89], which in turn enhances angiogenesis by promoting the recruitment of vascular cells in regions where FN fibres are denser.[90] Additionally, Wang et al. showed that breast cancer-conditioned cells would deposit not only denser but also thicker, stiffer and more unfolded FN fibres. Their thorough study indicates that the concomitant modification of multiple properties of FN fibres in the tumour microenvironment is responsible for altered FN signalling, in particular for the increased secretion of vascular endothelial growth factors (VEGF) that contributes to angiogenesis.[25] The same group later reported that these changes in structural and mechanical properties of FN fibres have repercussions on collagen type I matrix deposition (due to altered FN–collagen interactions), which consists of thicker and more aligned collagen fibres assembled in bundles, usually associated with tumour aggressiveness.[91]

1.7 Scope of the Thesis, Experimental Design and Materials

1.7.1 Scope of the Thesis

Although a significant amount of research has already been done on 3D soft hydrogels for tissue engineering purposes, there is still a need for tunable 3D ECM-mimicking scaffolds in cancer research. It is well known that both structural and mechanical features of the ECM fibrillar network contribute to cancer progression, but how these architectural and mechanical properties are related is still unclear. Therefore, it is important to thoroughly assess the entire spectrum of both elastic and viscoelastic features of fibrillar networks in order to establish correlations between their topology (architecture), conformation (secondary and tertiary protein structure) and mechanics.

In such a context, the goal of this thesis is to engineer and characterize a series of ECM-mimicking platforms composed of both collagen and FN, with material properties spanning from physiological to pathological (tumorous) tissues. Tunability of structural and mechanical properties will allow us (i) to establish a unique structure-mechanics relationship in the fibrillar networks, and in the future (ii) to investigate the effect of a variety of ECM cancer-associated alterations on cancer progression, in highly controlled and reproducible conditions.

Therefore, we will generate both ECM and cell-laden ECM scaffolds with controlled volume, mesh size, elasticity, and viscous (namely dissipative) characteristics. These tunable platforms will not only enable a better understanding of the critical link between ECM structure and mechanics but also help us in advancing our ultimate goal, which is the control of cellular functions. As such, these realistic ECM mimetics represent a valuable tool for biomaterials and biophysics research, with many potential applications in basic research, medical diagnosis, and tissue engineering.

1.7.2 Experimental Design

Based on previous work performed in our laboratory [92], we will first use a simple temperature-mediated casting method to fabricate three types of 3D collagen-fibronectin fibrillar scaffolds, either free of cells or loaded with cells, with varied materials properties. To evaluate the full range of mechanical characteristics of these ECM-mimicking scaffolds, we will have recourse to two different yet complementary techniques. First, all scaffolds will be subjected to increasing

compression forces using Dynamic Micromechanical device (home-made device) to extract their Young's moduli and assess their elasticity. We will then use a Rheometer (MCR 301 Anton Paar) to evaluate their full rheological behaviour when subjected to a large array of strains and strain rates. Methodology details are provided in Chapter 2.

1.7.3 Materials

Source of Collagen

Soluble rat-tail collagen I with a concentration of 4mg/ml (Advance Biomatrix) will be used to fabricate all 3D fibrillar scaffolds.

Source of Fibronectin

Bovine plasma fibronectin (Invitrogen, Thermo Fisher Scientific) will be diluted in 1x phosphate buffered saline (PBS) at a concentration of 1mg/ml for the stock solution and then used either during or after 3D collagen networks polymerization.

Source of Cells and Cell Culture

To study the effect of cells on the mechanics of our ECM-mimicking scaffolds, a highly aggressive breast cancer cell line, MDA-MB-231 (human breast adenocarcinoma) will be used. MDA-MB-231 cells will be cultured in Minimum Essential Medium Eagle-alpha modification (α-MEM) (Sigma Aldrich) including 10 vol% fetal bovine serum (FBS, Tissue Culture Biologics) and 1 vol% penicillin/streptomycin (Life Technologies) at 37°C in 5% CO_2. An average seeding density of 1.36×10^5 cells/mL will be used to generate cell-laden scaffolds.

1.8 References

1 Gattazzo F, Urciuolo A, Bonaldo P. 2014. Extracellular matrix: A dynamic microenvironment for stem cell niche. Biochim. Biophys. Acta - Gen. Subj. **1840**(8): 2506.

2 Ahearne M, Ahearne M. 2014. Introduction to cell – hydrogel mechanosensing.

3 Huijbers IJ, Iravani M, Popov S, Robertson D, Al-Sarraj S, Jones C, Isacke CM. 2010. A role for fibrillar collagen deposition and the collagen internalization receptor endo180 in glioma invasion. PLoS One. **5**(3): e9808.

4 Chan RW, Tayama N. 2002. Biomechanical effects of hydration in vocal fold tissues. Otolaryngol. neck Surg. Off. J. Am. Acad. Otolaryngol. Neck Surg. **126**(5): 528.

5 Chimich D, Shrive N, Frank C, Marchuk L, Bray R. 1992. Water content alters viscoelastic behaviour of the normal adolescent rabbit medial collateral ligament. J. Biomech. **25**(8): 831.

6 Järveläinen H, Sainio A, Koulu M, Wight TN, Penttinen R. 2009. Extracellular matrix molecules: potential targets in pharmacotherapy. Pharmacol. Rev. **61**(2): 198.

7 Walker C, Mojares E, Del Río Hernández A. Role of extracellular matrix in development and cancer progression. vol 192018.

8 Mosher DF. 1993. Assembly of fibronectin into extracellular matrix. Curr. Opin. Struct. Biol. **3**(2): 214.

9 Frantz C, Stewart KM, Weaver VM. 2010. The extracellular matrix at a glance. J. Cell Sci. **123**(Pt 24): 4195.

10 Ricard-Blum S. 2011. The collagen family. Cold Spring Harb. Perspect. Biol. **3**(1): a004978.

11 Hadjipanayi E, Mudera V, Brown RA. 2009. Guiding cell migration in 3D: A collagen matrix with graded directional stiffness. Cell Motil. Cytoskeleton. **66**(3): 121.

12 Chaudhuri O, Gu L, Darnell M, Klumpers D, Bencherif SA, Weaver JC, Huebsch N, Mooney DJ. 2015. Substrate stress relaxation regulates cell spreading. Nat. Commun. **6**: 1.

13 Engler AJ, Carag-krieger C, Johnson CP, Raab M, Tang H, Speicher DW, Sanger JW, Sanger JM, Discher E. 2009. Elasticity : Scar-Like Rigidity Inhibits Beating. Cell. **121**(Pt 22): 3794.

14 Ulrich TA, de Juan Pardo EM, Kumar S. 2009. The mechanical rigidity of the extracellular matrix regulates the structure, motility, and proliferation of glioma cells. Cancer Res. **69**(10): 4167.

15 Dalby MJ, Gadegaard N, Tare R, Andar A, Riehle MO, Herzyk P, Wilkinson CDW, Oreffo ROC. 2007. The control of human mesenchymal cell differentiation using nanoscale symmetry and disorder. Nat. Mater. **6**(12): 997.

16 Benoit DSW, Schwartz MP, Durney AR, Anseth KS. 2008. Small functional groups for controlled differentiation of hydrogel-encapsulated human mesenchymal stem cells. Nat.

Mater. **7**(10): 816.

17 Seo BR et al. 2020. Collagen microarchitecture mechanically controls myofibroblast differentiation. Proc. Natl. Acad. Sci. U. S. A. **117**(21).

18 Li T et al. 2005. The association of measured breast tissue characteristics with mammographic density and other risk factors for breast cancer. Cancer Epidemiol. Biomarkers Prev. **14**(2): 343.

19 Volokh K. Mechanics of Soft Materials. Springer Singapore, Singapore. 2019.

20 Provenzano PP, Inman DR, Eliceiri KW, Keely PJ. 2009. Matrix density-induced mechanoregulation of breast cell phenotype, signaling and gene expression through a FAK-ERK linkage. Oncogene. **28**(49): 4326.

21 Levental KR et al. 2009. Matrix crosslinking forces tumor progression by enhancing integrin signaling. Cell. **139**(5): 891.

22 Sun M et al. 2018. Effects of matrix stiffness on the morphology, adhesion, proliferation and osteogenic differentiation of mesenchymal stem cells. Int. J. Med. Sci. **15**(3): 257.

23 Engler AJ, Sen S, Sweeney HL, Discher DE. 2006. Matrix elasticity directs stem cell lineage specification. Cell. **126**(4): 677.

24 Sun M et al. 2018. Extracellular matrix stiffness controls osteogenic differentiation of mesenchymal stem cells mediated by integrin α5. Stem Cell Res. Ther. **9**(1): 1.

25 Wang K, Andresen Eguiluz RC, Wu F, Seo BR, Fischbach C, Gourdon D. 2015. Stiffening and unfolding of early deposited-fibronectin increase proangiogenic factor secretion by breast cancer-associated stromal cells. Biomaterials. **54**: 63.

26 Cameron AR, Frith JE, Cooper-White JJ. 2011. The influence of substrate creep on mesenchymal stem cell behaviour and phenotype. Biomaterials. **32**(26): 5979.

27 Salmeron-Sanchez M, Reboud J, Cooper JM, Cantini M, Bennett M, Roca-Cusachs P. 2018. Molecular clutch drives cell response to surface viscosity. Proc. Natl. Acad. Sci. **115**(6): 1192.

28 Chevallay B, Herbage D. 2000. Collagen-based biomaterials as 3D scaffold for cell cultures: applications for tissue engineering and gene therapy. Med. Biol. Eng. Comput. **38**(2): 211.

29 Wolf K, Alexander S, Schacht V, Coussens LM, von Andrian UH, van Rheenen J, Deryugina E, Friedl P. 2009. Collagen-based cell migration models in vitro and in vivo. Semin. Cell Dev. Biol. **20**(8): 931.

30 Burgeson RE, Nimni ME. 1992. Collagen types. Molecular structure and tissue distribution. Clin. Orthop. Relat. Res. (282): 250.

31 Elsdale T, Bard J. 1972. Collagen substrata for studies on cell behavior. J. Cell Biol. **54**(3): 626.

32 Prockop DJ, Kivirikko KI. 1995. Collagens: Molecular for Therapy. Proteins.

33 Hulmes DJS. 2002. Building collagen molecules, fibrils, and suprafibrillar structures. J. Struct. Biol. **137**(1–2): 2.

34 Lee CH, Singla A, Lee Y. 2001. Biomedical applications of collagen. Int. J. Pharm. **221**(1–2): 1.

35 Antoine EE, Vlachos PP, Rylander MN. 2015. Tunable collagen I hydrogels for engineered physiological tissue micro-environments. PLoS One. **10**(3): e0122500.

36 Hardy JG, Lin P, Schmidt CE. 2015. Biodegradable hydrogels composed of oxime crosslinked poly(ethylene glycol), hyaluronic acid and collagen: a tunable platform for soft tissue engineering. J. Biomater. Sci. Polym. Ed. **26**(3): 143.

37 Zhu C, Ma X, Xian L, Zhou Y, Fan D. 2014. Characterization of a co-electrospun scaffold of HLC/CS/PLA for vascular tissue engineering. Biomed. Mater. Eng. **24**(6): 1999.

38 Dallas SL, Chen Q, Sivakumar PBT-CT in DB. Dynamics of Assembly and Reorganization of Extracellular Matrix Proteins vol 75 Academic Press. pp 1–24.

39 Hörmann H. 1985. Fibronectin and phagocytosis. Blut. **51**(5): 307.

40 Potts JR, Campbell ID. 1996. Structure and function of fibronectin modules. Matrix Biol. **15**(5): 313.

41 Leahy DJ, Aukhil I, Erickson HP. 1996. 2.0 A crystal structure of a four-domain segment of human fibronectin encompassing the RGD loop and synergy region. Cell. **84**(1): 155.

42 Krammer A, Lu H, Isralewitz B, Schulten K, Vogel V. 1999. Forced unfolding of the fibronectin type III module reveals a tensile molecular recognition switch. Proc. Natl. Acad. Sci. **96**(4): 1351 LP.

43 Vogel V. 2006. mechanotransduction involving multimodular proteins: Converting Force into Biochemical Signals. Annu. Rev. Biophys. Biomol. Struct. **35**(1): 459.

44 Kubow KE, Vukmirovic R, Zhe L, Klotzsch E, Smith ML, Gourdon D, Luna S, Vogel V. 2015. Mechanical forces regulate the interactions of fibronectin and collagen I in extracellular matrix. Nat. Commun. **6**(1): 8026.

45 Singh P, Carraher C, Schwarzbauer JE. 2010. Assembly of Fibronectin Extracellular Matrix. Annu. Rev. Cell Dev. Biol. **26**(1): 397.

46 Smith ML, Gourdon D, Little WC, Kubow KE, Eguiluz RA, Luna-Morris S, Vogel V. 2007. Force-induced unfolding of fibronectin in the extracellular matrix of living cells. PLoS Biol. **5**(10): e268.

47 Constantine KL, Madrid M, Bányai L, Trexler M, Patthy L, Llinás M. 1992. Refined solution structure and ligand-binding properties of PDC-109 domain b. A collagen-binding type II domain. J. Mol. Biol. **223**(1): 281.

48 Bowditch RD, Hariharan M, Tominna EF, Smith JW, Yamada KM, Getzoff ED, Ginsberg MH. 1994. Identification of a novel integrin-binding site in fibronectin. Differential utilization by beta 3 integrins. J. Biol. Chem. **269**(14): 10856.

49 Mao Y, Schwarzbauer JE. 2005. Fibronectin fibrillogenesis, a cell-mediated matrix assembly process. Matrix Biol. **24**(6): 389.

50 To WS, Midwood KS. 2011. Plasma and cellular fibronectin: distinct and independent functions during tissue repair. Fibrogenesis Tissue Repair. **4**: 21.

51 Grinnell F. 1982. Fibronectin and wound healing. Am. J. Dermatopathol. **4**(2): 185.

52 Assoian RK, Schwartz MA. 2001. Coordinate signaling by integrins and receptor tyrosine kinases in the regulation of G1 phase cell-cycle progression. Curr. Opin. Genet. Dev. **11**: 48.

53 McDonald JA, Kelley DG, Broekelmann TJ. 1982. Role of fibronectin in collagen deposition: Fab' to the gelatin-binding domain of fibronectin inhibits both fibronectin and collagen organization in fibroblast extracellular matrix. J. Cell Biol. **92**(2): 485.

54 Foolen J, Shiu J-Y, Mitsi M, Zhang Y, Chen CS, Vogel V. 2016. Full-Length Fibronectin Drives Fibroblast Accumulation at the Surface of Collagen Microtissues during Cell-Induced Tissue Morphogenesis. PLoS One. **11**(8): e0160369.

55 Riande E. Polymer viscoelasticity stress and strain in practice. Marcel Dekker, New York. 2000.

56 Atala A. 2000. Tissue engineering of artificial organs. J. Endourol. **14**(1): 49.

57 Pilliar RM. 1991. Modern metal processing for improved load-bearing surgical implants. Biomaterials. **12**(2): 95.

58 Ratner BD, Bryant SJ. 2004. Biomaterials: where we have been and where we are going. Annu. Rev. Biomed. Eng. **6**: 41.

59 Ratner BD. Biomaterials science : an introduction to materials in medicine. Elsevier Academic Press, Amsterdam; Boston. 2004.

60 Langer R, Tirrell DA. 2004. Designing materials for biology and medicine. Nature. **428**(6982): 487.

61 Gong YY, Xue JX, Zhang WJ, Zhou GD, Liu W, Cao Y. 2011. A sandwich model for engineering cartilage with acellular cartilage sheets and chondrocytes. Biomaterials. **32**(9): 2265.

62 Cheng CW, Solorio LD, Alsberg E. 2014. Decellularized tissue and cell-derived extracellular matrices as scaffolds for orthopaedic tissue engineering. Biotechnol. Adv. **32**(2): 462.

63 Zitnay JL, Reese SP, Tran G, Farhang N, Bowles RD, Weiss JA. 2018. Fabrication of dense anisotropic collagen scaffolds using biaxial compression. Acta Biomater. **65**: 76.

64 Zhang YS, Khademhosseini A. 2017. Advances in engineering hydrogels. Science. **356**(6337).

65 Djabourov M, Leblond J, Papon P. 1988. Gelation of aqueous gelatin solutions. I. Structural investigation. J. Phys. **49**(2): 319.

66 Wichterle O, LÍM D. 1960. Hydrophilic Gels for Biological Use. Nature. **185**(4706): 117.

67 Morgan PB, Efron N, Helland M, Itoi M, Jones D, Nichols JJ, van der Worp E, Woods CA. 2010. Twenty first century trends in silicone hydrogel contact lens fitting: an international perspective. Cont. Lens Anterior Eye. **33**(4): 196.

68 Bonnier F, Keating ME, Wróbel TP, Majzner K, Baranska M, Garcia-Munoz A, Blanco A, Byrne HJ. 2015. Cell viability assessment using the Alamar blue assay: a comparison of 2D and 3D cell culture models. Toxicol. In Vitro. **29**(1): 124.

69 Cavo M, Fato M, Peñuela L, Beltrame F, Raiteri R, Scaglione S. 2016. Microenvironment complexity and matrix stiffness regulate breast cancer cell activity in a 3D in vitro model. Sci. Rep. **6**(January): 1.

70 Takagi A, Watanabe M, Ishii Y, Morita J, Hirokawa Y, Matsuzaki T, Shiraishi T. 2007. Three-dimensional cellular spheroid formation provides human prostate tumor cells with tissue-like features. Anticancer Res. **27**(1A): 45.

71 Desoize B. 2000. Multicellular resistance: a paradigm for clinical resistance? Crit. Rev. Oncol. Hematol. **36**(2–3): 193.

72 Fratzl P. 2008. Collagen: Structure and Mechanics, an Introduction. Collagen Struct. Mech. 1.

73 Gong Z et al. 2018. Matching material and cellular timescales maximizes cell spreading on viscoelastic substrates. Proc. Natl. Acad. Sci. U. S. A. **115**(12): E2686.

74 Ovijit Chaudhuri, Luo Gu, Darinka Klumpers, Max Darnell SA et al. 2016. Hydrogels with tunable stress relaxation regulate stem cell fate and activity. Nat. Mater. **15**(3): 10.

75 Cukierman E, Pankov R, Yamada KM. 2002. Cell interactions with three-dimensional matrices. Curr. Opin. Cell Biol. **14**(5): 633.

76 Lou J, Stowers R, Nam S, Xia Y, Chaudhuri O. 2018. Stress relaxing hyaluronic acid-collagen hydrogels promote cell spreading, fiber remodeling, and focal adhesion formation in 3D cell culture. Biomaterials. **154**: 213.

77 Nam S, Hu KH, Butte MJ, Chaudhuri O. 2016. Strain-enhanced stress relaxation impacts nonlinear elasticity in collagen gels. Proc. Natl. Acad. Sci. **113**(20): 5492.

78 Jordahl S et al. 2019. Engineered Fibrillar Fibronectin Networks as Three- Dimensional Tissue Scaffolds. **1904580**: 1.

79 Jaafar H, Sharif SET, Murtey M Das. 2014. Pattern of collagen fibers and localization of matrix metalloproteinase 2 and 9 during breast cancer invasion. Tumori. **100**(5): e204.

80 Balcioglu HE, van de Water B, Danen EHJ. 2016. Tumor-induced remote ECM network orientation steers angiogenesis. Sci. Rep. **6**: 22580.

81 Staunton JR, Vieira W, Fung KL, Lake R, Devine A, Tanner K. 2016. Mechanical properties of the tumor stromal microenvironment probed in vitro and ex vivo by in situ-calibrated optical trap-based active microrheology. Cell. Mol. Bioeng. **9**(3): 398.

82 Suresh S. 2007. Biomechanics and biophysics of cancer cells. Acta Biomater. **3**(4): 413.

83 Provenzano PP, Eliceiri KW, Campbell JM, Inman DR, White JG, Keely PJ. 2006. Collagen reorganization at the tumor-stromal interface facilitates local invasion. BMC Med. **4**(1): 38.

84 Jang M, Koh I, Lee JE, Lim JY, Cheong JH, Kim P. 2018. Increased extracellular matrix density disrupts E-cadherin/β-catenin complex in gastric cancer cells. Biomater. Sci. **6**(10): 2704.

85 Zhou ZH, Ji CD, Xiao HL, Zhao H Bin, Cui YH, Bian XW. 2017. Reorganized collagen in the tumor microenvironment of gastric cancer and its association with prognosis. J. Cancer. **8**(8): 1466.

86 Provenzano PP, Inman DR, Eliceiri KW, Knittel JG, Yan L, Rueden CT, White JG, Keely PJ. 2008. Collagen density promotes mammary tumor initiation and progression. BMC Med. **6**: 11.

87 Ohashi T, Kiehart DP, Erickson HP. 1999. Dynamics and elasticity of the fibronectin matrix in living cell culture visualized by fibronectin-green fluorescent protein. Proc. Natl. Acad. Sci. U. S. A. **96**(5): 2153.

88 Vogel V. 2018. Unraveling the Mechanobiology of Extracellular Matrix. Annu. Rev. Physiol. **80**(1): 353.

89 Wang JP, Hielscher A. 2017. Fibronectin: How its aberrant expression in tumors may improve therapeutic targeting. J. Cancer. **8**(4): 674.

90 Kim S, Bell K, Mousa SA, Varner JA. 2000. Regulation of angiogenesis in vivo by ligation of integrin alpha5beta1 with the central cell-binding domain of fibronectin. Am. J. Pathol. **156**(4): 1345.

91 Wang K, Wu F, Seo BR, Fischbach C, Chen W, Hsu L, Gourdon D. 2017. Breast cancer cells alter the dynamics of stromal fibronectin-collagen interactions. Matrix Biol. **60**–**61**: 86.

92 Asadishekari M. Design and Engineering of 3D Collagen-Fibronectin Scaffolds for Wound Healing and Cancer Research. MSc Thesis University of Ottawa 2018.

Chapter 2 – Theoretical Background and Methodology for Mechanical Characterization

2.1 Introduction to Mechanical Properties of Soft Tissues

Mechanical properties are intrinsic to every material, and they are usually closely related to the material structural organization. In biology, mechanical properties are also responsible for the proper physiological functions of tissues. In such a context, it is crucial to assess accurately *all* mechanical characteristics of biological tissues. In the case of soft tissues, at the heart of this thesis, their response to load and/or deformation may depend on prior loading, deformation and/or temperature history, which renders the task more tedious but also more interesting. This chapter focuses on (i) all mechanical characteristics of materials relevant in biology, and (ii) the different techniques available to evaluate such properties, with an emphasis on the case of compliant and soft tissues.

2.1.1 Elasticity

Elasticity is an intensive property of materials that shows a return to their initial state instantaneously upon removing the applied forces. Elastic moduli for solids are calculated from the ratio of stress to strain which can be described by the generalized Hooke's law. The coefficient that describes the ratio of the applied stress to the resultant strain is called Elastic Modulus or Young's Modulus (E), and it is given by:

$$E = \frac{\sigma}{\varepsilon}$$

The Young's modulus E with a unit of measurement in N/m^2 or Pa states that the stress response of an elastic material is independent of time. It is also defined as:

$$E = \frac{F\Delta L}{AL_0}$$

where strain (ε) is the stress-induced deformation in terms of relative displacement of the sample in some spatial dimension i.e., its elongation ΔL normalized by its initial value L_0 (ε is therefore dimensionless). Stress (σ) is defined as the applied force (load) F (N) divided by the cross-sectional area A (m^2), which is the area perpendicular to the load (cross-section of the specimen).

Many materials (not only polymers but also most metals) exhibit a S-shaped stress-strain curve, which consists of three different regions as shown in figure 2.1.

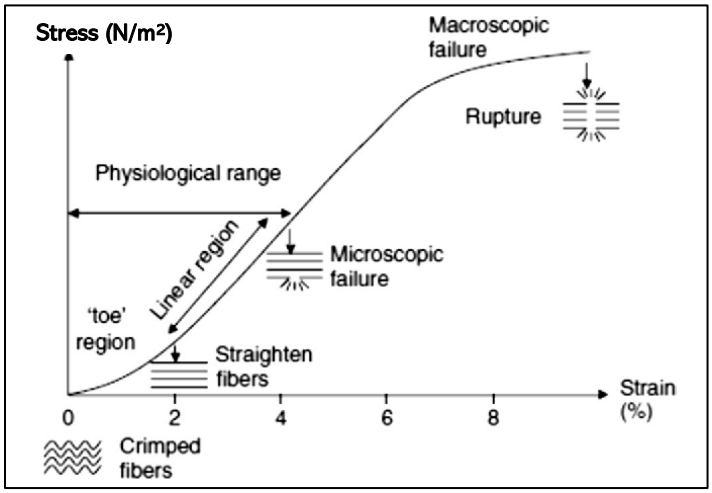

Figure 2.1 **Schematic of a stress-strain curve for tissues such as tendons, when subjected to tensile stresses.** Adapted from [1].

The first region is the "toe region", which corresponds to the initial uncrimping (and alignment) of fibres upon applying load. In the second (linear) region, fibres are straightened and start stretching. The slope of this linear portion is used to estimate Young's modulus of the material. In the third region, a further stretch of fibres causes molecular and fibrillar slippage, which eventually leads to macroscopic failure, i.e. failure of the entire specimen.[2] In the case of most soft biological tissues, the resistance to deformation typically increases when the applied stress increases, this phenomenon is called strain-stiffening and is illustrated by a J-shaped stress-strain curve.[3]

The above concept and properties relate to stresses applied perpendicularly to the material's 'long' axis (perpendicularly to the specimen cross-section), namely when stresses are applied either in tension or in compression, however, stresses are often applied parallelly to the specimen cross-section, which is the case of shear stresses. Shear stresses and the measurement of the shear modulus of materials are described in detail in Section 2.2.1.

2.1.2 Viscoelasticity

Biological tissues, especially soft tissues, display viscoelastic behaviour. Viscoelasticity is a combination of two elements with different responses including time-dependent strain (mean

dissipation) and retarded elastic deformation (or recovery) when undergoing deformation (or load removal). Applying load to viscoelastic materials leads to an increment of the system's energy. When viscoelastic materials store energy upon loading, part of the stored energy is returned upon unloading which refers to elasticity (see Section 2.1.1), but some of it is dissipated which represents the 'viscous' (mean dissipation) component. When the load is removed, rearrangements of macromolecules lower the total energy of the system and it reaches the equilibrium state.

Characteristic viscoelastic features of soft tissues are summarised in Figure 2.2. Figure 2.2.a displays the hysteresis phenomenon, where mechanical responses are not identical upon loading and unloading the tissue. As an important aspect of flow behaviour, hysteresis (dissipation loop) results from the gap between the input and the output energies. The input energy is the energy given to the specimen during loading while the output energy is the energy returned by the specimen during unloading. It shows a lack of equilibrium between the microstructure and the strain rate, often because the material is structurally fractured upon applying force. Therefore, when one wants to perform highly recommended 'equilibrium' (also called steady-state) measurements, it is essential to adjust the experimental process (e.g., strain rate) to minimize the hysteresis.

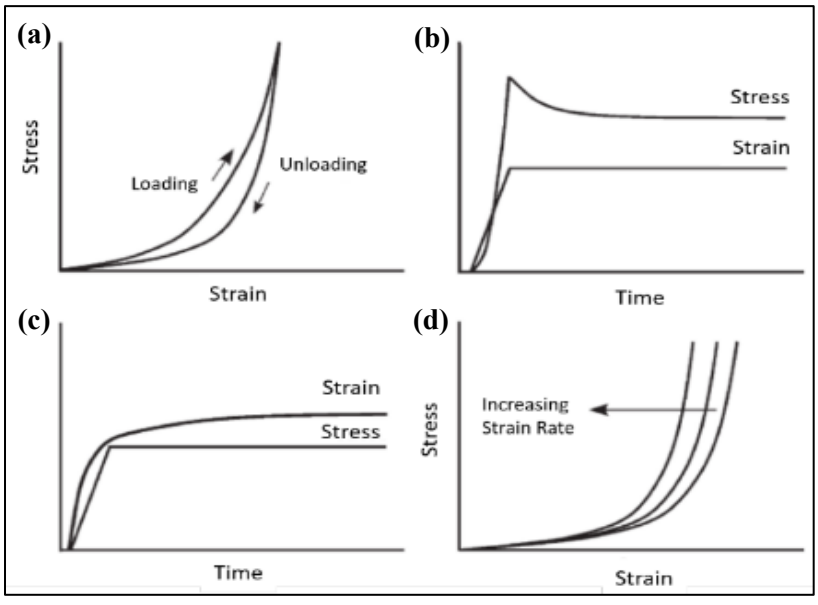

Figure 2.2 **Viscoelastic behaviour of soft tissues**. **a)** Hysteresis of a stress-strain profile upon loading and unloading of the tissue. **b)** Stress relaxation experiment in which stress decreases while the tissue is held at constant strain. **c)** Creep experiment in which strain increases while the tissue is held at constant (tensile) stress. **d)** Characteristic effect of strain rate on a stress-strain profile. Adapted from [4].

To characterize viscoelastic materials, creep and stress relaxation tests are the most common experiments. Imposing a constant deformation/strain on a polymer while following the resultant stress refers to stress relaxation (Figure 2.2.b). Applying a constant force/stress while following the deformation/strain refers to creep tests (Figure 2.2.c). Experimental characterization of biological soft tissues shows that stress-strain curves (i) are extremely sensitive to the rate at which the strain is applied (called strain rate, in other words, how fast we deform the system) and (ii) display relaxation phenomena. A well-known effect is the stiffening, i.e., the increase of stress-strain curve slope of soft tissues when the strain rate is increased, as clearly illustrated in Figure 2.2.d. The strain rate is therefore a significant variable that needs to be constantly monitored and controlled when characterizing soft tissues' mechanical behaviour.

Viscoelastic properties of materials may be linear (independent of imposed stress or strain) or nonlinear (dependent on applied stress or strain). The nonlinear viscoelastic response, for example, strain stiffening is a common attribute of soft tissues. All measurements need to be performed within the linear viscoelastic range (LVR), as only in this range can the relationship between molecular structure and viscoelastic material behaviour be properly determined. This theory explains how the microstructure of complex polymers and fluids is related to their rheological properties.

2.1.3 Poroelasticity

Besides viscoelasticity, which is usually associated with the reorientation/alignment of the (solid) polymer network when subjected to stresses, hydrogels show another well-known time-dependent behaviour: poroelasticity, which rather arises from the stress relaxation induced by the flow of fluid within the solid network. It is therefore essential to distinguish the contribution of poroelasticity to mechanical behaviour, especially when the considered solids are soft biological tissues (or matrices), which are highly porous structures immersed in fluids. Stress relaxation for hydrogels, such as collagen gels, is composed of two concurrent molecular processes.[5] On one hand, stretching, buckling, bending and slipping of the fibrils at interaction/contact points make conformational changes in the gel. It leads to gel network reorganization which represents its viscoelastic behaviour. On the other hand, the flow of interstitial fluids may slow the relative movement of the system or pressurize the system [6] resulting in poroelasticity.

Poroelasticity can be observed in any multiphase medium. It is not easy to differentiate viscoelastic and poroelastic behaviours in mechanical experiments. However, specific experimental protocols are employed to study these two phenomena independently, such as indentation and compression methods. As mentioned earlier, stress relaxation results from two concurrent yet individual responses that can be distinguished as follows. The poroelastic component of the relaxation depends on the sample characteristic length-scale, while the viscoelastic component of the relaxation is independent of the sample length-scale because the sample size is usually much bigger than the size of the pores present in the material.[7] Therefore when averaged load-relaxation curves for gels with different sizes are normalized by the individual sample size and plotted against time, the trends of each curve are offset in time.[8] The length-scale dependency of poroelastic mechanisms can also be determined from (simultaneous) analysis of multi-scale indentation experiments.[7]

2.1.4 Hydration Effect on Mechanical Properties

For most biological tissues (especially connective tissues), hydration is key to preserve their normal biochemical functions.[9] Several factors would dramatically affect the mechanical properties of soft tissues, e.g., ECM crosslinking [10] and/or hydration level. For example, dehydration of collagen matrices significantly reduces the spacing between fibres, which in turn alters both inter and intra-molecular bonds.[11] Studies on collagen fibrils revealed that their stiffness increases upon dehydration.[12] In fact, infrared reflection spectroscopy reveals that collagen hydrogen bonds strengthen and shorten during the dehydration process.[13] The hydration layer has also a structural function in keeping the critical spacing between collagen fibrils, as shown through Raman spectroscopy.[14]

2.2 Rheology

Rheology refers to the study of the flow of matter (mainly liquids but also solids) when it is subjected to stresses. It started with theories that describe so-called ideal materials. The first example is the description by Robert Hooke of ideal elastic solids, as described in Section 2.1.1. The second example is Isaac Newton's theory describing ideal liquids (also named Newtonian liquids), i.e., liquids whose viscosity stays constant, even though the shear rate (or strain rate) changes with time. Many materials such as soft materials are a combination of ideal solids (elastic) and ideal liquids (viscous) and are therefore called viscoelastic materials.

Various types of flow are recognized, as shown in Figure 2.3. Although all liquids flow when subjected to stresses, ideal and nonideal liquids behave differently.[15] A Newtonian (ideal) behaviour implies a linear relationship between stress and strain rate in the liquid and is the simplest flow behaviour encountered. Thus, in ideal liquids, the viscosity, η, remains constant, which means it is not affected by changes in the speed (rate) at which the liquid is flowing (see Section 2.2.1 for details). Instead, viscosity does not remain constant in nonideal liquids: in dilatant fluids, the viscosity increases with shear rate, also named shear-thickening effect, while in pseudoplastic liquids, the viscosity decreases with shear rate, also named shear-thinning effect.

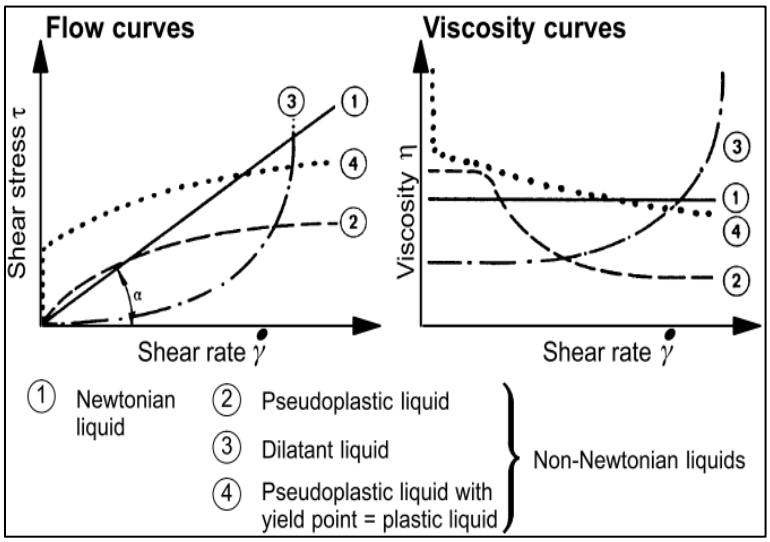

Figure 2.3 **Different types of flow behaviour in ideal and non-ideal liquids.** Adapted from [16].

Rheology is, therefore, crucial to quantify materials' viscoelasticity, and rheological experiments need to be performed using a wide range of time (rates) and deformation (strains) parameters to properly relate viscoelastic properties to the material structure. Soft materials exhibit complex deformations in response to mechanical loading, due to their heterogeneous internal structure and intricate composition of soft solids and fluids (filamentous polymers, and other supra-molecular). Stress and strain relationships are functions of time, direction, and length of deformation. Several controlled techniques including stress relaxation, creep and oscillatory shear can be performed to assess rheological characteristics. Depending on the viscoelastic models used, rheological results are expressed in terms of relaxation modules, creep conformance, storage and loss modulus, respectively.

2.2.1 Shear

Shear forces are at the heart of rheology to evaluate the flow behaviour of materials. Shear can be illustrated using a simple two-plates model (Figure 2.4). A shear force is defined as a force applied to the face of a sample sandwiched between two opposing plates, which direction is parallel to these plates.[15] The elastic deformation induced by this shear force is called shear deformation. The ratio of shear stress to shear strain is called the shear modulus, *G*, which describes the resistance of the solid against deformation:

$$G = \frac{\tau}{\gamma}$$

where τ is the shear stress (shear force per unit area) in Pa, and γ is the shear strain, i.e., the relative change in length (dimensionless). The coefficient G is the constant of proportionality called shear modulus (Pa). Similar to the Young modulus *E*, shear modulus *G* is an intensive elastic property of solids. The difference is that *G* deals with the ability of a specimen to elastically deform when stresses are applied 'along' the specimen surface (shear force), instead of perpendicularly to the specimen surface (compressive or tensile force) as described for *E* in Section 2.1.1. This relation can also be written as:

$$G = \frac{Fh}{A\Delta x}$$

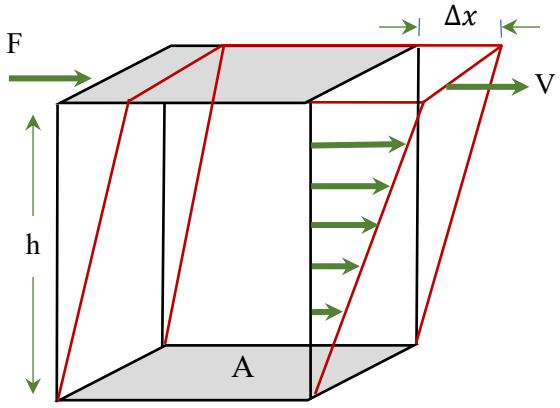

Figure 2.4 **Schematic of two plate model showing the velocity distribution of flow.** [17]

where the shear stress $\tau = F/A$ (in contrast to normal stress seen in Section 2.1.1, here the cross-sectional area *A* of the object is *in the plane parallel* to the shear force *F*), and the shear strain $\gamma = \Delta x/h$ is the finite deformation along the shear force *F*, i.e., the elongation Δx normalized by the

initial specimen thickness h (in contrast to normal strain ε seen in Section 2.1.1, here the characteristic length h is perpendicular to the shear force F). γ is dimensionless.

When the deformation continues over time, i.e., when the material flows at a relative speed V, the shear deformation Δx increases with time. The rate at which Δx increases is the shear (strain) rate, or simply the shear rate. Therefore, under flow, the shear stress τ becomes proportional to the shear rate ($\dot{\gamma}$) of the planes, which is equal to V/h. As explained in more detail in Section 2.2.2, the coefficient of proportionality between shear stress and shear (strain) rate defines the viscosity η:

$$\eta = \frac{\tau}{\dot{\gamma}}$$

Oscillatory shear stresses are widely used to characterize the viscoelastic behaviour of soft materials.[18] In such method, cyclic (sinusoidal) strains are applied over time, which causes sinusoidal shear forces in the sample, measured as the resulting stress response. The relative contributions of both viscous and elastic responses are assessed using this technique.

In the oscillatory shear technique, shear strain (in small amplitude oscillatory shear) can be written as:

$$\gamma(t) = \gamma_0 sin\omega t$$

And the stress response of viscoelastic material under oscillatory shear stress is given by:

$$\sigma = \sigma_0 \sin(\omega t + \delta),$$

which can also be written as:

$$\sigma = G'\gamma_0 \sin\omega t + G''\gamma_0 cos\omega t$$

where the shear stress consists of two components: a modulus G′ which is in phase ($\delta = 0°$) with the shear strain and a modulus G″ which is out of phase (δ = 90°) with the shear strain.

In large amplitude oscillatory shear, which provides the information of nonlinear viscoelasticity of materials, the sinusoidal shear strain is defined as:

$$\gamma(t) = \gamma_0 e^{iwt}.$$

Using oscillatory mode within the linear viscoelasticity range, the shear strain and shear stress are related by:

$$\sigma(t) = G^* \gamma(t)$$

where G* is the complex modulus (also called dynamic modulus), which is composed of in-phase and out of phase components with the oscillating strain as:

$$G^*(\omega) = G'(\omega) + iG''(\omega)$$

The storage modulus, G', corresponds to the elastic element of viscoelastic materials, in other words, it represents the ability of materials to store energy in the elastic structure of the sample. The loss modulus, G″, describes the ability of a material to dissipate energy in the structure of the material. In the linear viscoelastic region (LVR) or the adequately small strain regime, both storage and loss moduli are independent of strain.

2.2.2 Viscosity

Fluids at a given strain rate will show resistance to flow known as viscosity (η). This flow resistance is caused by the interaction between various molecules in a fluid i.e., the internal friction between molecules. Accordingly, the viscosity is defined as:

$$\eta = \frac{\sigma}{\dot{\gamma}}$$

where σ is the shear stress and $\dot{\gamma}$ the shear (strain) rate.

Additionally, we define the frequency-dependent complex viscosity (η*) as:

$$\eta^*(\omega) = \frac{G^*(\omega)}{i\omega}$$

$$\eta^*(\omega) = \eta'(\omega) - i\eta''(\omega)$$

$$\eta^*(\omega) = G''/\omega - G'/\omega$$

The complex viscosity is defined by the relation between complex stress and strain rate. The storage modulus is related to the elastic component of viscosity (η″) while the loss modulus is related to the viscous component of viscosity (η′), known as dynamic viscosity.

2.2.3 Loss Factor

In oscillatory experiments, the ratio of loss modulus to storage modulus ($G''(\omega)/G'(\omega)$) is called the loss factor, or tan (δ), and it provides the relative degree of energy dissipation (damping) in the material. For ideal (pure) elastic materials, $\delta = 0°$ (stress is in phase with strain) and

G"(ω)→0, while for ideal (pure) viscous materials $\delta = 90°$ (stress is out of phase with strain) and G'(ω)→0.

2.3 Tools for Elasticity and Viscoelasticity Measurements

2.3.1 Dynamic Mechanical Analyzer

Several tools are available to evaluate the mechanics of soft tissues depending on the mechanical properties that need to be assessed along with the samples' size and geometry. In this thesis, we used a custom-built Dynamic Mechanical Analyzer (DMA) to evaluate the elasticity of all our fibrillar collagen-FN scaffolds, in the absence and/or presence of cells. More specifically, small increments of strain were cyclically applied to each sample using the two parallel plates configuration of the DMA device. To assess sample stiffness, Young's modulus was calculated during compression with the help of LabVIEW software. Importantly, each sample was kept hydrated in PBS at all times during measurements. Force-indentation curves were recorded by compressing the material in small strain increments up to the desired final strain, and at a constant velocity. All measurements were carried out under cyclic dynamic loading and velocity fixed at 25μm/s. This velocity value was chosen because it was the most suitable rate available to ensure quasi-static measurements and limit viscous effects (lowest velocity were also tested but they led to highly noisy data that were discarded). Prior to each measurement, up to 35% pre-strain was applied to secure the sample within the loading cell and ensure its direct and homogeneous contact with both loading plates. Samples were then deformed up to 25% strain. To restrict heating of the surfaces and consequent dehydration of the sample, ice packed gels were placed all around the device. Next, seven consecutive loading cycles were applied to each sample and all seven force-indentation curves were recorded. Because the elastic modulus of the gels estimated from the first compression cycle was systematically far higher than that obtained from the following six cycles (likely due to the loss of excess PBS in the gels), it was discarded. Finally, the force-indentation data of the six compressive cycles left were averaged and converted to stress-strain data and the elastic modulus (E) for each gel was extracted as the slope of the stress-strain plots in the low-strain regime (2–8 % strain).

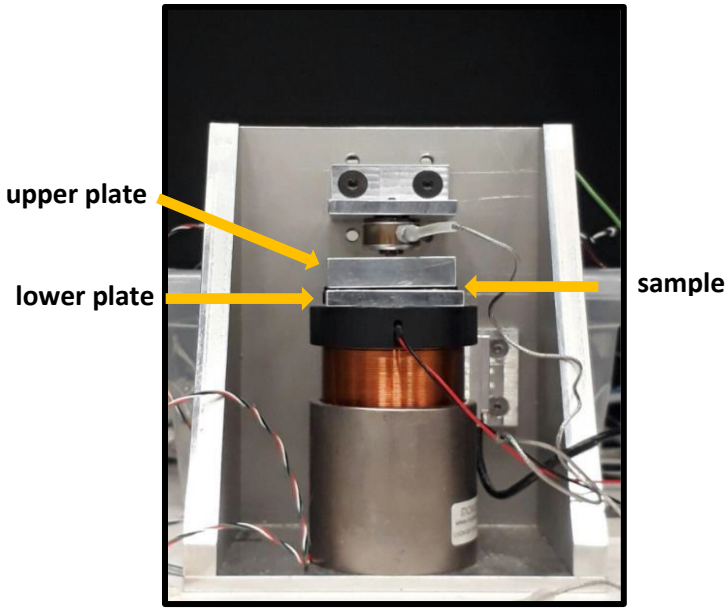

Figure 2.5 **A custom-built Dynamic Mechanical Analyzer (DMA)** to perform Young's modulus measurements in compression.

2.3.2 Rheometer

A rheometer is an instrument with great functionality used to measure a vast array of viscoelastic characteristics of solids, semi-solids and fluids. It can measure the viscosity and elasticity of Newtonian and non-Newtonian materials under a broad variety of conditions, as opposed to a viscometer that is limited in its use for the measurement of the viscous flow behaviour of fluids. Viscoelasticity, yield stress, creep compliance and stress relaxation are some of the most important properties that can be determined with a rheometer.

A rheometer allows one to measure torque, deflection angle and speed. Shear parameters such as shear stress and shear strain rate are obtained from measurements of torque and flow rate, at each measuring point. The application of torque on the top plate results in rotational shear stress on the surface, which provides the resultant strain or strain rate (shear rate). Two types of rheology testing can be performed: rotational tests and/or oscillatory tests. While the measuring bob turns in only one direction in rotational tests, it oscillates around its axis in oscillatory tests.

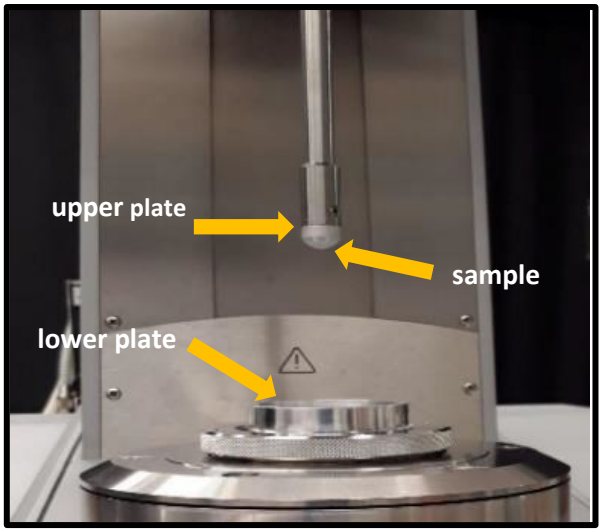

Figure 2.6 **A parallel plate rheometer (MCR 301 Anton Paar).** The picture shows the experimental configuration prior to the final approach, i.e., before subsequent gluing of the sample to the lower plate, which ensures pure rotational shear within the sample and no slippage at the interface with the lower plate.

Different testing geometries are available depending on the type of rheometers, including the plate-plate, cone plate, and Couette geometry. In this thesis, we used a strain-controlled rheometer (SSC: an operation mode for pre-setting the deflection) with plate-plate geometry, in which each sample was placed (glued) between two strictly parallel stainless steel sandblasted plates, separated by a gap of controllable size, and constantly immersed in PBS.

Amplitude sweep tests were first systematically performed on each sample to determine their linear viscoelastic regime (LVR). In these tests, the frequency was held constant while the amplitude of the deformation was increased across two orders of magnitude of strains (namely from 0.1% to 10% strain). The LVR ensures that neither the storage modulus (G′) nor the loss modulus (G″) shows a dependency on the applied strain. Based on these amplitude sweeps (repeated at three different frequencies) and the LVR we determined, in this thesis, we report a large amount of highly reproducible data obtained at a strain rate of 0.1 (1/s) and a strain of 0.25%. As detailed in Chapter 4, all trends were similar at lower frequencies and/or higher strains, unless stated otherwise.

Next, we operated frequency sweep tests within the LVR regime to quantify all relevant rheology time-dependent characteristics of each sample. During frequency sweeps, the amplitude/strain was set to 0.25% and the strain rate was decreased from 10 to 0.1 (1/s). Storage

modulus, loss modulus, viscosity, as well as loss factor were determined from those measurements. These experiments were repeated at both 0.5% and 1% strains, but only results showing a different trend than that obtained at 0.25% are reported and discussed in the main body of this thesis. All data acquired at 0.5% and 1% strains are reported in the Appendix.

2.4 Statistical Analysis

One-way ANOVA with Tukey post hoc test and Student's t-test were used to analyze statistical significance between conditions using GraphPad Prism (GraphPad Software, California USA). All presented values are the mean ± the standard deviation of our data. Statistical significance * refers to $P < 0.05$, ** to $P<0.01$, *** to $P<0.001$, **** to $P<0.0001$.

2.5 References

1 Catterall RCF. 1968. An Introduction to Biomechanics. J. Bone Joint Surg. Br. **50-B**(1): 242.

2 Silver FH, Ebrahimi A, Snowhill PB. 2002. Viscoelastic properties of self-assembled type I collagen fibers: molecular basis of elastic and viscous behaviors. Connect. Tissue Res. **43**(4): 569.

3 Levin SM. 2015. Tensegrity: the new biomechanics. Oxford Textb. Musculoskelet. Med. (January 2006): 150.

4 Michael Lee J. 2006. Tissue Mechanics. Wiley Encycl. Biomed. Eng.

5 Hu Y, Suo Z. 2012. Viscoelasticity and poroelasticity in elastomeric gels. Acta Mech. Solida Sin. **25**(5): 441.

6 Chandran PL, Barocas VH. 2004. Microstructural mechanics of collagen gels in confined compression: poroelasticity, viscoelasticity, and collapse. J. Biomech. Eng. **126**(2): 152.

7 Strange DGT, Fletcher TL, Tonsomboon K, Brawn H, Zhao X, Oyen ML. 2013. Separating poroviscoelastic deformation mechanisms in hydrogels. Appl. Phys. Lett. **102**(3).

8 Anirudh QW, Michelle CM, Zhao LOX. 2014. Separating viscoelasticity and poroelasticity of gels with different length and time scales. **30**: 20.

9 Wachtel E, Maroudas A. 1998. The effects of pH and ionic strength on intrafibrillar hydration in articular cartilage. Biochim. Biophys. Acta. **1381**(1): 37.

10 Xu B, Chow M-J, Zhang Y. 2011. Experimental and Modeling Study of Collagen Scaffolds with the Effects of Crosslinking and Fiber Alignment. C T Lim, ed.Int. J. Biomater. **2011**: 172389.

11 Mogilner IG, Ruderman G, Grigera JR. 2002. Collagen stability, hydration and native state. J. Mol. Graph. Model. **21**(3): 209.

12 McDaniel DP, Shaw GA, Elliott JT, Bhadriraju K, Meuse C, Chung KH, Plant AL. 2007. The stiffness of collagen fibrils influences vascular smooth muscle cell phenotype. Biophys. J. **92**(5): 1759.

13 George A, Veis A. 1991. FTIRS in H2O demonstrates that collagen monomers undergo a conformational transition prior to thermal self-assembly in vitro. Biochemistry. **30**(9): 2372.

14 Leikin S, Parsegian VA, Yang WH, Walrafen GE. 1997. Raman spectral evidence for hydration forces between collagen triple helices. Proc. Natl. Acad. Sci. U. S. A. **94**(21): 11312.

15 Jorge TDS, Polachini TC, Dias LS, Jorge N, Telis-romero J. 2015. Rheological characterization. **16**(5): 390.

16 Schramm G. A practical approach to rheology and rheometry. Gebrueder Haake, Karlsruhe.

1994.

17 Luminita Iordan A. Rheological properties of biological materials : from cell suspensions to tissues, Phd Thesis Joseph Fourier University 2008.

18 Edwards S. 1988. Dynamics of polymeric liquids vol. 1, fluid mechanics, edited by R. B. Bird, R. C. Armstrong and 0. Hassager, Wiley Interscience, New York, 1987. ISBN 0-471-80245-X. Vol. 2, Kinetic theory, edited by R. B. Bird, C. F. Curtiss,. Br. Polym. J. **20**(3): 299.

Chapter 3 - Structural and Dynamic Mechanical Analysis of 3D fibrillar Collagen-Fibronectin Scaffolds

3.1 Introduction

The ECM plays a significant role in development, regeneration, but also diseases such as cancer.[1] More specifically, the structural and morphological characteristics of the ECM such as the structure of its individual components (fibre diameter, length), the conformation of proteins, and the overall matrix density all influence cellular behaviour.[2] Additionally, the biomechanical characteristics of the ECM, including stiffness, regulate key cellular functions such as proliferation, differentiation, survival and migration.[3][4] Both the structure and the mechanics of the ECM are noticeably altered in disease conditions.[2][5] During tumour growth, the ECM of the tumour microenvironment is gradually remodelled by tumour cells, which affects its physical properties and impacts the efficacy of treatment.[4] In most cancers, the tumour tissue (comprising both cells and their ECM) is stiffer than its healthy counterpart.[6][7][8]

Studies have demonstrated that increased ECM deposition, in particular, upregulation of collagen (COL) and fibronectin (FN) deposition [9][10] results in increased density and stiffness of the ECM, which is associated with increased risk of breast cancer.[7][11] To investigate cellular behaviour, recent research has focused widely on studying COL type I (COL-I), a major fibrillar ECM component and FN, the prominent glycoprotein in the ECM.[12][13] COL fibres' thickness and alignment are increased in tumour tissues, suggesting a stiff environment and indicating a tumour-promoting stroma [14], while they are curly and compliant in healthy ECM networks.[15] In the early stages of growth, the tumour tissue was also reported to comprise dense, stiff, and unfolded FN, which in turn results in altered COL-I deposition and promotes tumour vascularisation.[16]

In tissue engineering, COL scaffolds of varied microstructures have been utilized to provide substrates with tunable mechanical properties. The varied microstructure was achieved by control of (i) COL concentration, (ii) polymerization temperature and/or (iii) pH.[17] More specifically, monitoring the above-mentioned parameters allows one to control COL scaffold density (pore size), topology of individual COL fibres, such as fibre length, diameter, and overall fibre alignment.[18]

In this thesis, we used a temperature-mediated casting method developed by a former student in the Gourdon group to fabricate 3D fibrillar COL-FN networks with constant protein concentrations yet different microarchitectures.[19] The temperature was the main parameter used to control the rate of COL gelation and get fibrillar scaffolds of varied density and fibre morphology. As a result, we generated three types of COL-FN scaffolds with low, medium and high network density, and we correlated their microarchitecture with their mechanical characteristics. All scaffolds were fabricated both in the absence (cell-free) and in the presence (cell-laden) of breast cancer cells. In this chapter, we first introduce scaffolds' structural information obtained via fluorescence microscopy, then we present in detail the mechanical analysis we performed using a custom-built Dynamic Mechanical Analyzer (DMA) to estimate scaffolds' Young's modulus (E) in compression mode.

3.2 Materials and Methods

3.2.1 Fabrication and Microstructure of Fibrillar Collagen-Fibronectin Scaffolds Prepared Using Warm/Cold Casting Technique

Cell-free scaffolds: To fabricate the 3D fibrillar scaffolds, we used a temperature-mediated or cold/warm casting method previously implemented in the Gourdon lab. Briefly, a neutralization solution was mixed to a Rat Tail Collagen solution (4 mg/ml) (both from Advanced BioMatrix) in a 1:9 ratio to obtain a neutralized COL solution at a final concentration of 2.88 mg/ml. The COL solution was then added to either pre-cooled or pre-warmed 96 well-plates. A final volume of 150 µl per well was necessary to obtain 1.0 mm thick COL scaffolds. In the cold-casting method, the solution was added in pre-cooled well plates and gradually polymerized under temperatures ranging from 4°C (fridge for 15 min), 15°C (environmental chamber for 15 min) to 37°C (incubator for 24 h), which ensured a slow rate of polymerization to generate thick COL fibrils. In the warm-casting method, the solution was added in pre-warmed well plates and rapidly polymerized at 37°C, which resulted in thin COL fibrils. In this thesis, we also fabricated a third sample under conditions that were intermediate between cold- and warm-casting. Importantly, all well plates and solutions were kept on ice during preparation. Finally, to better mimic the ECM, FN was added to the COL solutions at various stages of the gel preparation up to a final

concentration of 0.2 mg/ml.[19] (FN was added to Well A, Well C, and Well E at t=0, t=20 and t=30 minutes, respectively).

Cell-laden scaffolds: Next, we fabricated similar COL-FN fibrillar scaffolds with pre-embedded cells. MDA-MB-231 cells (breast cancer cells) were incubated in α-MEM (Sigma Aldrich) including 10 vol% fetal bovine serum (FBS, Tissue Culture Biologicals) and 1 vol% penicillin/streptomycin (Life Technologies) at 37°C in 5% CO2. The neutralized COL solution was mixed with 10 µl MDA-MB-231 cells solution containing 100,000 cells to get final cell-embedded COL gels with approximately 2.004×10^4 cells per well. Cell-laden scaffolds were prepared via the same cold/warm casting method as cell-free scaffolds, without any use of chemical crosslinking.

The microstructure of the resulting cell-free scaffolds was assessed via laser scanning confocal microscopy performed by Javad Eslami, a graduate student currently in the Gourdon group. Fluorescence images (acquired in reflectance mode for COL and conventional fluorescence mode for previously labelled FN) and associated structural analysis are summarized in Figure 3.1. From these data, first, it is important to note that all scaffolds exhibit a fibrillar structure rather than a porous hydrogel morphology and that both COL (red) and FN (green) are present and able to form distinct networks of fibres. Next, it is clear that warm-casted scaffolds (well E) exhibit dense networks composed of short and thin fibres, while cold-casted scaffolds (well A) show sparse networks composed of long and thick fibres. Intermediate temperature casted scaffolds (well C) display intermediate matrix properties in terms of pore/mesh size and fibre topology, which indicates that we are able to *gradually* tune the scaffolds' microstructure by accurately controlling the rate of COL gelation.

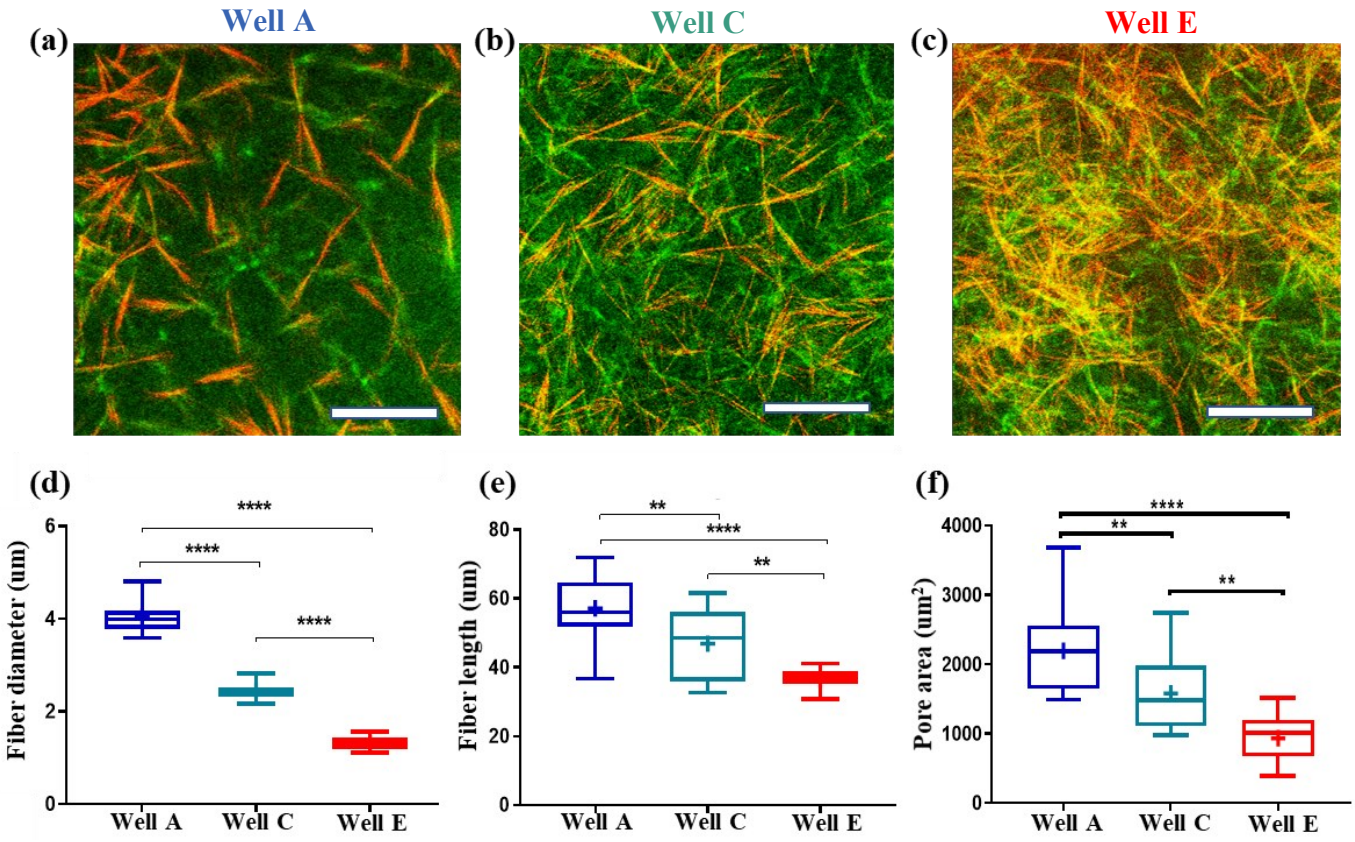

Figure 3.1 **Microstructure analysis of cell-free collagen-fibronectin scaffolds**. Combined reflectance and conventional fluorescence confocal images (Red: COL-I, Green: FN) of scaffolds engineered at varied polymerization temperatures: **a)** Well A (Cold-casted); **b)** Well C (Intermediate temperature casted); **c)** and Well E (Warm-casted). Fibre topology and scaffold mesh size **d)** Average COL fibre diameter for Well A (4.0±0.3 µm), Well C (2.5±0.2 µm) and Well E (1.3±0.1 µm); **e)** Average COL fibre length for Well A (57.1±10.7 µm), Well C (46.9±10.2 µm) and Well E (36.4±3.3 µm). **f)** Average COL-FN scaffold pore/mesh size for Well A (2196±587 µm^2), Well C (1580±525 µm^2) and Well E (934.7±336 µm^2). (n=15 for all wells) (**P<0.01, ***P<0.001, ****P<0.0001; One-way ANOVA). Mean±SD. Scale bars = 50 µm. Data obtained by courtesy of Javad Eslami.

3.2.2 Dynamic Mechanical Analysis of 3D Fibrillar Collagen-Fibronectin Scaffolds

In this thesis, Young's moduli of all COL-FN scaffolds were measured in compression via a custom-made Dynamic Mechanical Analyzer (DMA), as shown in Figure 2.5. Prior to each experiment, all scaffolds were incubated for 24 h at 37°C, immersed in PBS. After 24 h, each sample was mounted on the DMA and placed between two parallel plates. Excess PBS was removed, and the initial cross-sectional area (A_0) was measured prior to compression. All measurements were carried out under cyclic dynamic loading, at velocity of 50 µm/s, 25 µm/s and

10 µm/s. However, our data acquired at 50 µm/s clearly displayed significant viscous effects (highly hysteretic), and those acquired at 10 µm/s were extremely noisy. Therefore, in this thesis, we only report the data obtained at 25 µm/s, as this velocity was the most suitable rate available to ensure quasi-static measurements and limit viscous effects. We also tested two different maximum levels of applied strain, namely 25% and 50%. However, as 50% strain showed clear signs of plastic deformation, we restricted our compressive measurements to 25% maximum strain. Importantly, up to 35% pre-strain was applied before acquiring force-indentation data, to ensure proper (homogeneous) direct contact of each sample with the DMA loading plates. To restrict heating of the plates and consequent dehydration of the sample, ice packed gels were placed all around the device. The applied force (F) was measured while monitoring sample deformation/indentation (L_i) up to 25% strain, using LabVIEW software. Overall, seven consecutive loading cycles were applied to each sample and all seven force-indentation curves were recorded.

The force-indentation data of the six successive compressive cycles were converted to engineering stress-strain data, i.e., using initial cross-sectional area A_0 for stress calculations (Figure 3.2.a). The Young's modulus (E) was calculated as the slope of the stress-strain curve ($E=\sigma/\varepsilon= FL_0/A_0(L_i-L_0)$) over the low-strain or elastic regime (2–8%), as shown in Figure 3.2.b. Note that these strain values do not include the 35% pre-strain. Importantly, to determine L_0 as the initial (uncompressed) sample thickness, we used the indentation (L_i) at which we could clearly see an onset of repulsive forces while the two compression plates were brought towards each other.

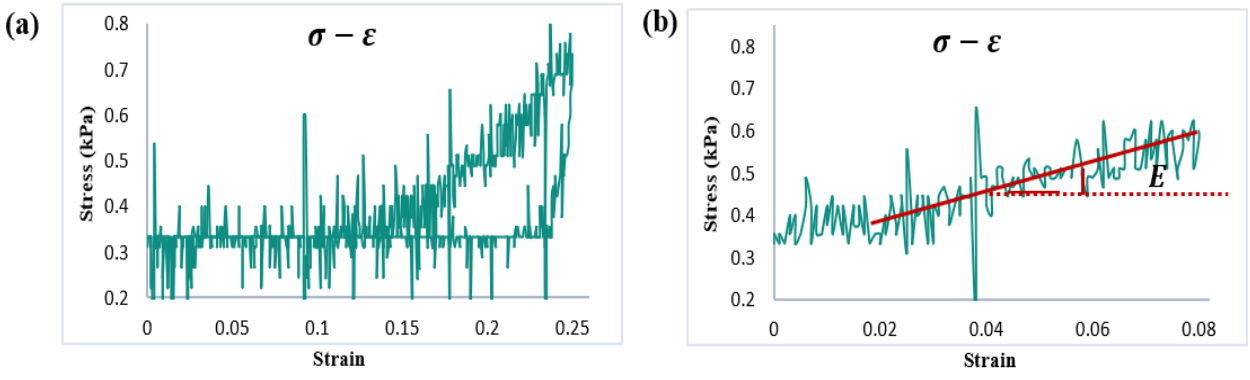

Figure 3.2 **Young's modulus measurements in compression**. **a)** Average converted stress-strain curve obtained when a sample was compressed under cyclic force up to 25% strain, at a constant velocity of 25 µm/s. **b)** Elastic modulus (E) as calculated from the initial slope of engineering stress-strain ($\sigma= \varepsilon E$) in the low strain 2–8% regime.

3.3 Results

3.3.1 Experimental Analysis of Collagen-Fibronectin Network Mechanical Properties in Cell-Free Scaffolds

We first characterized the mechanical properties of our COL-FN scaffolds in the absence of cells. In brief, we prepared three types of scaffolds using temperature-mediated casting that allowed us to gradually monitor their microstructure, from low-density networks (Well A) to high-density networks (Well E).[17] We then analyzed how these different microarchitectures affected the elastic moduli of the scaffolds using DMA compression tests. As shown in Figure 3.3, our data indicate that there was no difference in Young's compressive modulus between cold and warm-casted scaffolds, regardless of their clear different microarchitecture. Although there may exist a trend suggesting higher mean stiffness values for Well C and Well E, i.e., for higher density scaffolds, no statistical difference was measured over 6 to 8 samples per condition. Overall, our data indicate that, regardless of polymerization temperature and associated structure, the bulk stiffness of all our COL-FN cell-free scaffolds was around ~ 2 kPa, which is in the compliant range of rigidities found in native tissues. In human tissues, the elastic modulus of COL networks varies from hundreds Pa (compliant brain tissue) up to a few GPa (stiff cortical bone).[20]

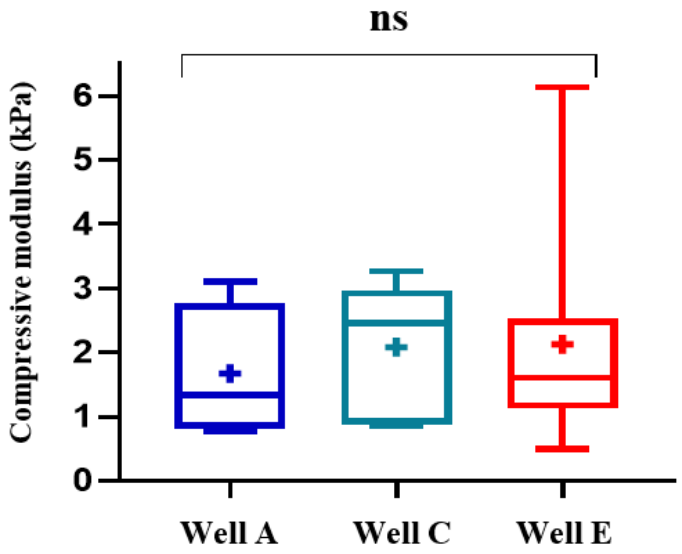

Figure 3.3 **Compressive moduli of fibrillar COL-FN scaffolds in the absence of cells**. The results show that there is no significant difference between compressive Young's moduli measured on Well A (E=1.67±0.98 kPa) (n=6), Well C (E=2.08±1.03 kPa) (n=8) and Well E (E=2.13±1.75 kPa) (n=8), in the absence of cells. (One-way ANOVA) Mean ± SD. ns: no significance, P>0.05.

3.3.2 Experimental Analysis of Collagen-Fibronectin Network Mechanical Properties in Cell-Laden Scaffolds

Next, we repeated our DMA compressive measurements on the three types of COL-FN scaffolds, in presence of cells, using the same experimental parameters. According to our results summarized in Figure 3.4, even when scaffolds are loaded with cells, no difference in Young's compressive modulus was observed. Therefore the presence of cells did not affect significantly scaffolds' stiffness, even though warm-casted and cold-casted samples exhibited different microstructure (data not shown).[19] Overall our findings indicate that the mean stiffness of all three cell-laden scaffolds was approximately 2 kPa, i.e., similar to that of cell-free scaffolds measured in Section 3.3.1.

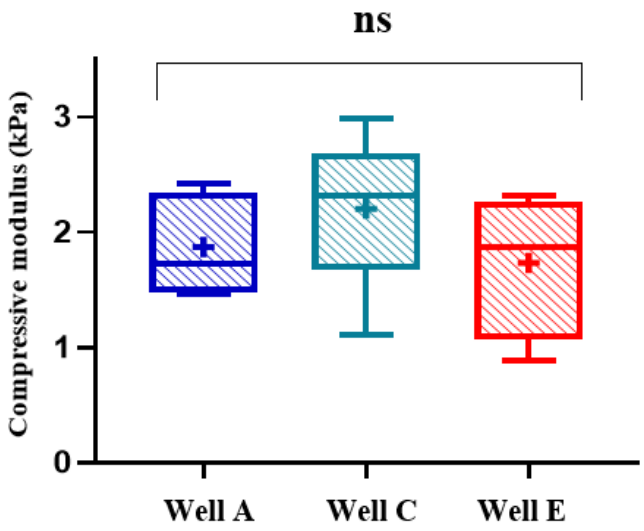

Figure 3.4 **Compressive moduli of fibrillar COL-FN scaffolds in the presence of cells**. The results show that there is no significant difference between compressive Young's moduli measured on Well A (E=1.87±0.44 kPa) (n=5), Well C (E=2.20±0.68 kPa) (n=5) and Well E (E=1.73±0.63 kPa) (n=4). (One-way ANOVA) Mean ± SD. ns: no significance, P>0.05.

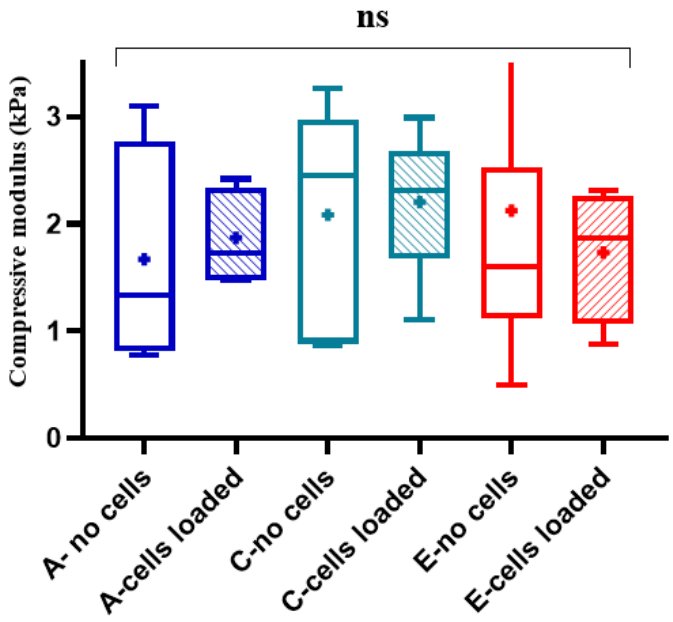

Figure 3.5 **Comparison of compressive moduli between cell-free and cell-laden fibrillar COL-FN scaffolds (24h)**. Although there is no significant difference in compressive moduli between scaffolds, the presence of cells tends to (i) increase stiffness of Wells A and C, and (ii) decrease stiffness of Well E. (One-way ANOVA). ns: no significance, P>0.05.

To determine whether a trend existed between cell-free and cell-loaded scaffolds fabricated in the same conditions, Figure 3.5 displays all compressive moduli we obtained via DMA. When having a closer look at these data, it can be noticed that the presence of cells tended to increase the stiffness of sparse scaffolds (Well A and Well C), however, it tended to decrease that of the denser scaffold (Well E). This trend suggests that cells may affect the mechanics of scaffolds in different ways, depending on their ability to establish cell-matrix interactions and on the type of interactions they can engage with the matrix, which are both highly dependent on the mesh size of the surrounding scaffold.

3.4 Discussion

Mechanical characterization of soft/compliant gels is complex because it is highly sensitive to testing conditions. In particular, the magnitude of the prestress applied can lead to significant variations in water content over time, and/or irreversible (plastic) gel deformations, even under small preloads.[21] In fact, a major source of uncertainty in our results is related not only to the intrinsic nature of soft tissues that are quite rough and behave anisotropically but also to the variations of prestress from sample to sample (as initial thickness and/or hydration level differed

slightly for all samples). Additionally, the initial contact of the confining plates with sample's surfaces at the beginning of each experiment (needed to determine the initial uncompressed sample thickness L_0) could lead to significant variations in prestress, resulting in different strain ranges over which compressive moduli were estimated.[22][23][24] Finally, although we attempted to restrict the dehydration process during measurements, it may also have occurred and may have altered the structure of the COL networks, likely increasing their density [17] which in turn would increase their stiffness while recording consecutive force-indentation data.[25] Despite these experimental challenges, in this Chapter, we presented a reproducible set of data obtained on a total of 22 cell-free scaffolds and 14 cell-laden scaffolds. Our results clearly indicate no significant difference in Young's modulus between scaffolds, regardless of their varied microstructure and regardless of their cell content. However, we could identify interesting cell-induced trends that we are discussing below, in terms of density-dependent cell-matrix interactions.

ECM structural and mechanical features are crucial factors for regulating tumour progression. Changing the polymerization temperature (at constant COL concentration) leads to alterations in fibril topology [26] and overall gel architecture, as well as to variations in elasticity of both the full matrix and the individual fibres.[27] Thanks to previous work in our laboratory, a temperature-casting method had already been determined to control the rate of COL gelation and generate two types of scaffolds with different microarchitectures.[19] Since systematic mechanical characterization was the main scope of the present thesis, we simply implemented the existing method to fabricate a series of ECM-mimicking platforms with gradual structural changes. As seen in Figure 3.1, we successfully generated a series of three mixed scaffolds composed of both COL and FN fibres with gradual changes in microstructure, from dense (small mesh size) networks composed of short and thin fibres (rapidly polymerized warm-casted samples) to sparse (large mesh size) networks composed of long and thick fibres (slowly polymerized cold-casted samples). In addition, those COL-FN scaffolds were fabricated either cell-free or loaded with breast cancer cells.

The characterization of scaffolds mechanical properties was achieved via the measurement of compressive moduli, using a Dynamic Mechanical Analyzer (DMA) to record stress-strain profiles on all scaffolds, in quasi-static conditions (velocity of 25 μm/s) and maximum applied strain of 25%. Despite obvious structural differences seen between the various scaffolds, no significant difference in Young's modulus was measured between them, regardless of the presence

of cells. Overall, all scaffolds were found highly compliant, exhibiting similar bulk stiffness of ~2 kPa, as encountered in soft native tissues.[20] These results are discussed in more detail in the last paragraph.

The comparison between cell-free and cell-loaded scaffolds revealed an interesting trend. While the presence of cells tended to increase the stiffness of sparse scaffolds (Well A and Well C), it had the opposite effect on the denser scaffold (Well E). This trend suggests that cells affect the mechanics of scaffolds in different ways, depending on scaffold/matrix mesh size because they likely establish different types (and number) of cell-matrix interactions. First, cells might play different 'mechanical' roles: in a dense fibrillar network such as Well E, cells might act as spacers between the tightly packed fibres, hence lowers network mesh size and overall stiffness; instead, in a sparse fibrillar network such as Well A, cells could localize within the initially large pores, reducing pores' size, which would contribute to increasing overall network stiffness. Note that increased cell-matrix interactions would also lead to thickening of individual fibres and/or inter-fibres crosslinking, which would as well promote stiffening of initially low-density networks. Nevertheless, neither these cell-induced changes nor the structural differences between scaffolds were able to significantly affect their elastic moduli, which suggests that, either our technique was not sensitive enough because our macro-scale stiffness measurements would eclipse micro-scale stiffness variations present in the scaffolds [28] or our quasi-static testing in compression mode was *per se* not adapted to capture these structural and mechanical variations (mainly because we would primarily detect poroelastic effects, i.e., water migration in and out of the porous scaffolds during cyclic compressions).

3D fibrillar matrix characteristics are the nonlinear combination not only of the stiffness of the entire macroscopic scaffold but also the stiffness of individual fibres. It has been reported that, although Young's modulus of individual COL and fibrin fibres can be in the MPa range, a COL gel can be much more compliant, i.e., in Pa or kPa range.[29] Such difference arises because overall gel's bulk mechanical properties depend on overall fibre architecture and mesh/scaffold organization rather than on the strength and stiffness of individual fibres.[30][31] In particular, macro-scale compressive testing studies were reported to be more efficient at characterizing bulk architectural features like density, which may not reflect accurately local structural variations and actual stiffness experienced by cells at the micro-scale.[32] The mechanical response to strain of reconstituted matrices was shown to be a combination of water migration, individual fibre

architecture and overall network reorganization.[30] In hydrogels under compression, it is the fluid phase that initially bears the applied loads. COL networks show very distinct behaviours depending on the type of stress they are subjected to, namely whether they are under compression, tension or shear.[33] Compared to stretching, bending is a soft mode of deformation.[34] Our gels contain a very small solid fraction of fibres (fluid volume fraction is much higher) resulting in weak resistance to compression. The bulk mechanical properties, therefore, are generally independent of the strength of individual fibres.[30] Additionally, some studies demonstrated that macro-scale compressive testing does not allow to detect variations between aligned and random fibres [28][35][36], although the architecture of COL fibres has an important effect on the overall mechanical properties of COL matrices.[37] Our results are in agreement with those reported by Seo et al., showing that despite differences in the structure of several COL gels, bulk compressive testing was useless to establish distinct mechanical properties between those gels.[38][39]

Therefore, in an effort to distinguish varied mechanical properties of our scaffolds in a more appropriate and physiological manner (cells usually deform their surrounding ECM by applying tension and releasing stresses through collective reorganization of the ECM), in Chapter 4, we examined whether the variations in network microstructure could modulate the rheological properties of our COL-FN scaffolds, when subjected to shear stresses.

3.5 Conclusions

We used a temperature casting method to generate a series of both cell-free and cell-loaded scaffolds made of the two prominent ECM proteins COL and FN. Our structural analysis revealed that all scaffolds had a fibrillar structure and that we successfully achieved gradual control of their microstructure, from dense networks composed of short and thin fibres to sparse networks composed of long and thick fibres. Our mechanical analysis using a costume-built macroscopic Dynamic Mechanical Analyzer (DMA) in compression mode did not allow us to establish a correlation between scaffold architecture and mechanics, as all our measurements indicated a compressive Young's modulus of circa 2 kPa, regardless of microstructure and cells' content.

Such compliant tunable scaffolds potentially offer excellent ECM-mimicking substrates to monitor cell functions in large volumes and over long cell culture times within scaffolds of varied microarchitectures (able to mimic either physiological or pathological microenvironments).

However, as mechanical properties of ECM have been widely recognized to guide cellular activity that can lead to cancer progression [7], it is crucial to establish a clear correlation between the microstructure and the mechanics of those scaffolds, at both macroscopic and microscopic scales. In such a context, Chapter 4 is dedicated to the comprehensive analysis of the rheological properties of all COL-FN scaffolds when subjected to shear stress, which better simulates cells' interactions with their surrounding ECM.

3.6 References

1 Insua-Rodríguez J, Oskarsson T. 2016. The extracellular matrix in breast cancer. Adv. Drug Deliv. Rev. **97**: 41.

2 Malandrino A, Mak M, Kamm RD, Moeendarbary E. 2018. Complex mechanics of the heterogeneous extracellular matrix in cancer. Extrem. Mech. Lett. **21**: 25.

3 Gattazzo F, Urciuolo A, Bonaldo P. 2014. Extracellular matrix: A dynamic microenvironment for stem cell niche. Biochim. Biophys. Acta - Gen. Subj. **1840**(8): 2506.

4 Dong C, Zahir N, Konstantopoulos K. Biomechanics in Oncology. Springer International Publishing. 2018.

5 Dalby MJ, Gadegaard N, Tare R, Andar A, Riehle MO, Herzyk P, Wilkinson CDW, Oreffo ROC. 2007. The control of human mesenchymal cell differentiation using nanoscale symmetry and disorder. Nat. Mater. **6**(12): 997.

6 Zanotelli MR, Reinhart-King CA. 2018. Mechanical Forces in Tumor Angiogenesis. Adv. Exp. Med. Biol. **1092**: 91.

7 Li T et al., 2005. The association of measured breast tissue characteristics with mammographic density and other risk factors for breast cancer. Cancer Epidemiol. Biomarkers Prev.**14**(2):343.

8 Volokh K. Mechanics of Soft Materials. Springer Singapore, Singapore. 2019.

9 Sapudom J, Rubner S, Martin S, Kurth T, Riedel S, Mierke CT, Pompe T. 2015. The phenotype of cancer cell invasion controlled by fibril diameter and pore size of 3D collagen networks. Biomaterials. **52**(1): 367.

10 Conklin MW, Eickhoff JC, Riching KM, Pehlke CA, Eliceiri KW, Provenzano PP, Friedl A, Keely PJ. 2011. Aligned collagen is a prognostic signature for survival in human breast carcinoma. Am. J. Pathol. **178**(3): 1221.

11 Provenzano PP, Inman DR, Eliceiri KW, Knittel JG, Yan L, Rueden CT, White JG, Keely PJ. 2008. Collagen density promotes mammary tumor initiation and progression. BMC Med. **6**: 1.

12 Goyal R, Vega ME, Pastino AK, Singh S, Guvendiren M, Kohn J, Murthy NS, Schwarzbauer JE. 2017. Development of hybrid scaffolds with natural extracellular matrix deposited within synthetic polymeric fibers. J. Biomed. Mater. Res. A. **105**(8): 2162.

13 Lowe CJ, Reucroft IM, Grota MC, Shreiber DI. 2016. Production of Highly Aligned Collagen Scaffolds by Freeze-drying of Self-assembled, Fibrillar Collagen Gels. ACS Biomater. Sci. Eng. **2**(4): 643.

14 Robertson C. 2016. The extracellular matrix in breast cancer predicts prognosis through composition, splicing, and crosslinking. Exp. Cell Res. **343**(1): 73.

15 Fang M, Yuan J, Peng C, Li Y. 2014. Collagen as a double-edged sword in tumor progression. Tumour Biol. J. Int. Soc. Oncodevelopmental Biol. Med. **35**(4): 2871.

16 Wang K, Andresen Eguiluz RC, Wu F, Seo BR, Fischbach C, Gourdon D. 2015. Stiffening and unfolding of early deposited-fibronectin increase proangiogenic factor secretion by breast cancer-associated stromal cells. Biomaterials. **54**: 63.

17 Gautieri A, Vesentini S, Redaelli A, Buehler MJ. 2011. Hierarchical structure and nanomechanics of collagen microfibrils from the atomistic scale up. Nano Lett. **11**(2): 757.

18 Yang YL, Leone LM, Kaufman LJ. 2009. Elastic moduli of collagen gels can be predicted from two-dimensional confocal microscopy. Biophys. J. **97**(7): 2051.

19 Asadishekari M. Design and Engineering of 3D Collagen-Fibronectin Scaffolds for Wound Healing and Cancer Research. MSc Thesis University of Ottawa 2018.

20 Swift J, Discher DE. 2014. The nuclear lamina is mechano-responsive to ECM elasticity in mature tissue. J. Cell Sci. **127**(Pt 14): 3005.

21 Holzapfel GA. Biomechanics of Soft Tissue. pp 1057–71.

22 Tirella A, Mattei G, Ahluwalia A. 2014. Strain rate viscoelastic analysis of soft and highly hydrated biomaterials. J. Biomed. Mater. Res. - Part A. **102**(10): 3352.

23 Ayyildiz M, Cinoğlu S, Basdogan C. 2015. Effect of normal compression on the shear modulus of soft tissue in rheological measurements. J. Mech. Behav. Biomed. Mater. **49**.

24 Vahabi M, Sharma A, Licup AJ, van Oosten ASG, Galie PA, Janmey PA, MacKintosh FC. 2016. Elasticity of fibrous networks under uniaxial prestress. Soft Matter. **12**(22): 5050.

25 Mogilner IG, Ruderman G, Grigera JR. 2002. Collagen stability, hydration and native state. J. Mol. Graph. Model. **21**(3): 209—213.

26 Wolf K et al. 2013. Physical limits of cell migration: Control by ECM space and nuclear deformation and tuning by proteolysis and traction force. J. Cell Biol. **201**(7): 1069.

27 Doyle AD, Carvajal N, Jin A, Matsumoto K, Yamada KM. 2015. Local 3D matrix microenvironment regulates cell migration through spatiotemporal dynamics of contractility-dependent adhesions. Nat. Commun. **6**.

28 Taufalele P V., VanderBurgh JA, Muñoz A, Zanotelli MR, Reinhart-King CA. 2019. Fiber alignment drives changes in architectural and mechanical features in collagen matrices. PLoS One. **14**(5): 1.

29 Guthold M, Liu W, Sparks EA, Jawerth LM, Peng L, Falvo M, Superfine R, Hantgan RR, Lord ST. 2007. A comparison of the mechanical and structural properties of fibrin fibers with other protein fibers. Cell Biochem. Biophys. **49**(3): 165.

30 Pedersen JA, Swartz MA. 2005. Mechanobiology in the third dimension. Ann. Biomed. Eng. **33**(11): 1469.

31 Lee B, Zhou X, Riching K, Eliceiri KW, Keely PJ, Guelcher SA, Weaver AM, Jiang Y. 2014. A three-dimensional computational model of collagen network mechanics. PLoS One. **9**(11): 1.

32 Bordeleau F et al. 2017. Matrix stiffening promotes a tumor vasculature phenotype. Proc. Natl. Acad. Sci. U. S. A. **114**(3): 492.

33 Licup AJ, Münster S, Sharma A, Sheinman M, Jawerth LM, Fabry B, Weitz DA,

MacKintosh FC. 2015. Stress controls the mechanics of collagen networks. **112**(31).

34 Abhilash AS, Baker BM, Trappmann B, Chen CS, Shenoy VB. 2014. Remodeling of fibrous extracellular matrices by contractile cells: Predictions from discrete fiber network simulations. Biophys. J. **107**(8): 1829.

35 Fraley SI, Wu PH, He L, Feng Y, Krisnamurthy R, Longmore GD, Wirtz D. 2015. Three-dimensional matrix fiber alignment modulates cell migration and MT1-MMP utility by spatially and temporally directing protrusions. Sci. Rep. **5**(September): 1.

36 Shannon GS, Novak T, Mousoulis C, Voytik-Harbin SL, Neu CP. 2015. Temperature and concentration dependent fibrillogenesis for improved magnetic alignment of collagen gels. RSC Adv. **5**(3): 2113.

37 Jansen KA, Licup AJ, Sharma A, Rens R, MacKintosh FC, Koenderink GH. 2018. The Role of Network Architecture in Collagen Mechanics. Biophys. J. **114**(11): 2665.

38 Seo BR et al. 2020. Collagen microarchitecture mechanically controls myofibroblast differentiation. Proc. Natl. Acad. Sci. U. S. A. **117**(21).

39 Carey SP, Kraning-Rush CM, Williams RM, Reinhart-King CA. 2012. Biophysical control of invasive tumor cell behavior by extracellular matrix microarchitecture. Biomaterials. **33**(16): 4157.

Chapter 4 - Rheological Analysis of the Viscoelastic Properties of 3D Fibrillar Collagen-Fibronectin Scaffolds

4.1 Introduction

The ECM is a highly heterogeneous and compliant scaffold, which, as most native tissues, exhibits viscoelastic characteristics rather than pure elastic behaviour.[1] Viscoelastic materials combine both elastic and viscous responses to applied loads and deformations. ECM viscoelasticity was reported to play an active role in regulating cellular activities including focal adhesion formation, cell spreading, and cell migration.[2][3] As different studies have found, changes in the viscous properties of native tissues (besides elasticity) are associated with disease progressions, such as fibrosis and breast cancer.[2][4] Recent research focusing on cells cultured in hydrogels with controlled viscous and elastic properties suggested that viscosity could be as important as stiffness in regulating cell spreading and proliferation, under specific conditions.[5][6][7][8] Interestingly, it was reported that cell-ECM adhesions and cell spreading are enhanced by viscosity on compliant substrates, whereas they are insensitive to viscosity on stiff substrates.[6][7][8]

Different approaches have been proposed to modulate the viscoelastic properties of hydrogels for cell culture, either by adjusting the architecture of the polymer [9] and/or the type of crosslink.[7] As discussed in Chapter 3, the COL-FN scaffolds we fabricated via the temperature casting exhibited varied fibrillar microarchitecture, nevertheless, elasticity measurements performed in compression with the DMA failed to fully characterize their full mechanical properties, only indicating an average Young's compressive modulus of circa 2 kPa for all scaffolds, regardless of their structure and/or cellular contents. COL hydrogels are known to be substantially viscoelastic, mainly because they consist of proteins self-assembled over weak bonds [9][10] and therefore display a significant frequency-dependent mechanical behaviour. Additionally, native tissues are often subjected to complex shear forces rather than to simple compressive or tensile stresses. In such a context, Chapter 4 is dedicated to the comprehensive analysis of the rheological properties of all COL-FN scaffolds when subjected to shear stress,

which better simulates the microenvironmental stresses pattern of native tissues, and particularly the interactions of cells with their surrounding ECM.

When a rheometer is used to perform dynamic shear tests on gels, it allows one to determine a whole range of bulk (macroscopic) viscoelastic properties, among which gel storage (elasticity) and loss (viscosity) moduli.[11][12] Cell behaviour is indeed affected by gel loss modulus, as it was reported that COL-based hydrogels with similar storage moduli but greater loss moduli would promote MSC cell spreading and differentiation.[7]

In this chapter, we aimed at fully characterizing the bulk rheological properties of our cell-free and cell-laden COL-FN scaffolds, when subjected to shear stresses. We were able to determine the elastic (G′, storage modulus) and viscous (G″, loss modulus) components of the scaffolds' viscoelastic properties. Besides their ability to quantify viscosity, bulk rheology measurements also showed much higher sensitivity to detect variations in elasticity in our scaffolds.[11][13][14]

4.2 Materials and Methods

4.2.1 Fabrication of Fibrillar Collagen Scaffolds with Varied Microstructure Using Warm/Cold Cast Technique

To fabricate COL-FN scaffolds for viscoelastic characterization using our rheometer, we adapted the temperature-casting cell-free and cell-laden protocols [15] described in Chapter 3 in order to scale up sample size. Final samples' dimensions were as follows: 2 mm in thickness and 12 mm in diameter, which would correspond to the dimensions of the plates used to confine and shear the scaffolds in the rheometer.

Cell-free scaffolds: Briefly, a neutralization solution was mixed to a Rat Tail Collagen solution (4 mg/ml) (both from Advanced BioMatrix) in a 1:9 ratio to obtain a neutralized COL solution at a final concentration of 2.88 mg/ml. The COL solution was then added to either pre-cooled or pre-warmed homemade Teflon moulds. A final volume of 350 µl per mould was necessary to obtain 2.0 mm thick COL scaffolds. In the cold-casting method, the solution was added in pre-cooled moulds and gradually polymerized under temperatures ranging from 4°C (fridge for 15 min), 15°C (environmental chamber for 15 min) to 37°C (incubator for 24h), which ensured a slow rate of polymerization to generate thick COL fibrils. In the warm-casting method,

the solution was added in pre-warmed moulds and rapidly polymerized at 37°C, which resulted in thin COL fibrils. In this thesis, we also fabricated a third sample under conditions that were intermediate between cold- and warm-casting. Importantly, all moulds and solutions were kept on ice during preparation. Finally, to better mimic the ECM, FN was added to the COL solutions at various stages of the gel preparation up to a final concentration of 0.2 mg/ml.[15]

Cell-laden scaffolds: Next, we fabricated similar COL-FN fibrillar scaffolds with pre-embedded cells. MDA-MB-231 cells (breast cancer cells) were incubated in α-MEM (Sigma Aldrich) including 10 vol% fetal bovine serum (FBS, Tissue Culture Biologicals) and 1 vol% penicillin/streptomycin (Life Technologies) at 37°C in 5% CO2. The neutralized COL solution was mixed with 10µl MDA-MB-231 cells solution containing 100,000 cells to get final cell-embedded COL gels with approximately 4.8×10^4 cells per mould/sample. Cell-laden scaffolds were prepared via the same cold/warm casting method as cell-free scaffolds, without any use of chemical crosslinking.

Cell-free and cell-laden scaffolds microstructure: Our structural analysis presented at length in Chapter 3 revealed that all COL-FN scaffolds contained fibrillar networks instead of a jelly porous morphology, exhibiting gradual variations in their microstructure (overall density and topology) from sparse networks composed of long and thick fibres (Well A) to dense networks composed of short and thin fibres (Well E).[15]

4.2.2 Rheological Measurement of 3D Fibrillar Collagen-Fibronectin Scaffolds

The rheological properties of all scaffolds were assessed using a parallel plate rheometer (MCR 301 Anton Paar) with circular plates of 12mm in diameter, as shown in Figure 2.6. The surface of the plates was sandblasted to increase surface roughness and improve adhesion with the glue to secure the (extremely slippery) scaffolds. Prior to testing, excess PBS was carefully removed from the samples, which were left highly hydrated. Because full shear (instead of partial shear) is crucial to determine accurately the viscoelastic properties of the material, it is important to avoid any slippage at the sample/plates interface, which would lead to arbitrarily reduced dissipation (viscosity).[16] Thus, all scaffolds were glued to both the upper plate and the lower plate (after approach) using Permabond Instant Adhesive 102 Medium Viscosity General Purpose Glue. The first step consisted of lowering the upper plate (to which the sample had already been

glued) to an approximate distance of ~1.65 mm from the lower plate (to which the sample was glued in situ). Experiments were conducted at room temperature 23–24℃, during which DI water was carefully added on the periphery of the sample to prevent sample dehydration. We then systematically followed the same experimental protocol to analyze all COL-FN scaffolds, as described below.

Oscillatory strain (amplitude) sweep tests were first performed on each sample to determine their linear viscoelastic regime (LVR). In these tests, frequency was held constant while amplitude of the deformation was increased across two orders of magnitude of strains (namely from 0.1% to 10% strain). The LVR ensures that neither the storage modulus (G') nor the loss modulus (G'') shows a dependence on the applied strain. Based on all amplitude sweeps (performed at three different frequencies) and the LVR that was determined in each case, in this thesis, we only report data obtained at a strain rate of 0.1 (1/s) and a strain of 0.25%, considered within the LVR (Figure 4.1.b). Next, we operated frequency sweep tests within the LVR regime to quantify all relevant rheology time-dependent characteristics of each sample. During frequency sweeps, the amplitude/strain was set to 0.25% and the strain rate was decreased from 10 to 0.1 (1/s). Storage modulus and loss modulus (Figure 4.1.c), but also complex viscosity and loss factor ($\tan\delta$) (Figure 4.1.d) were determined from those measurements. All frequency sweep experiments were repeated at both 0.5% and 1% strains, but only results showing a different trend than that obtained at 0.25% are reported and discussed in Chapter 4 of this thesis. All data acquired at 0.5% and 1% strains are reported in the final Appendix.

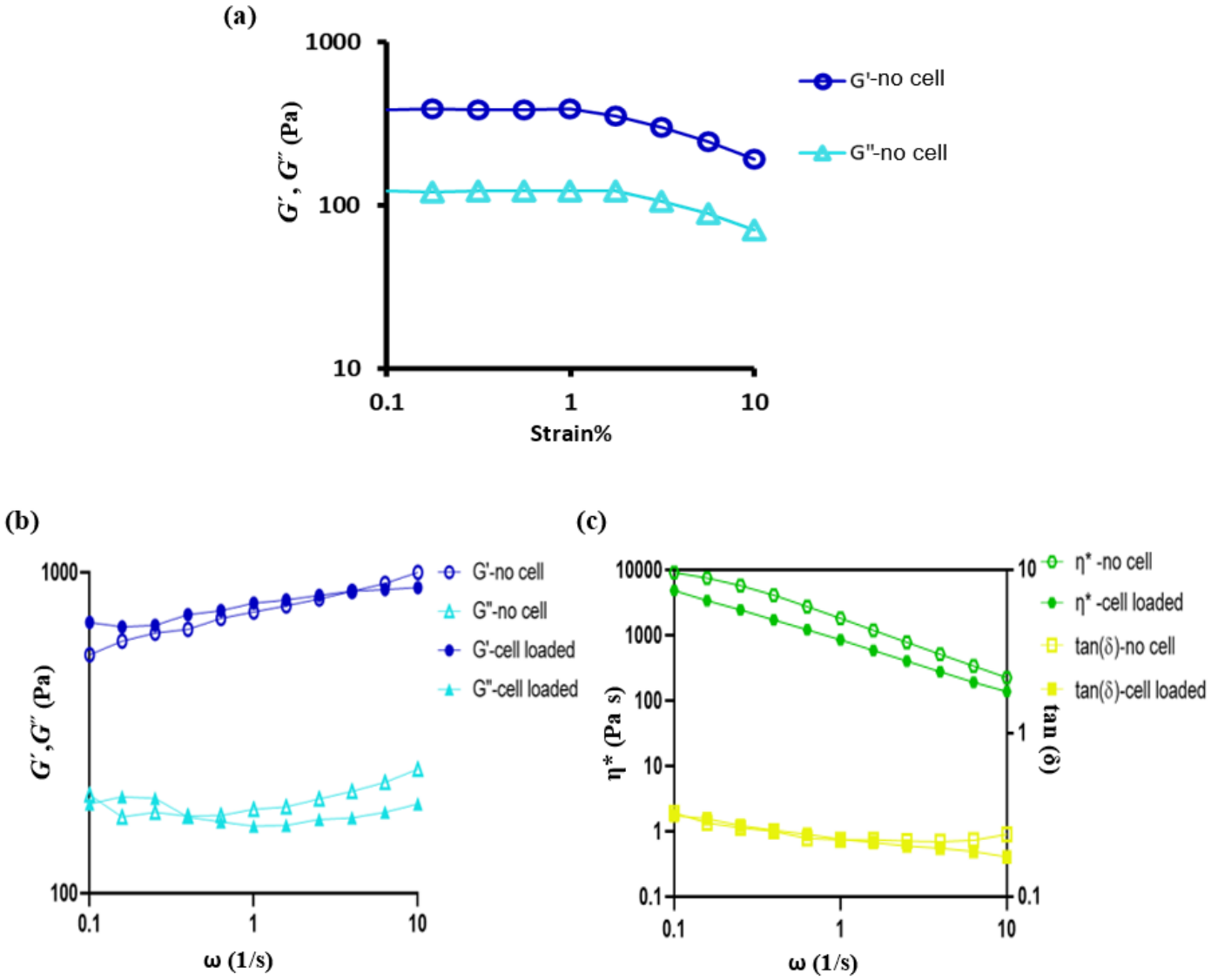

Figure 4.1 **Oscillatory shear test performed on cell-free and cell-loaded COL-FN scaffolds with a rheometer**. **a)** Strain (amplitude) sweep performed at a constant strain rate of 0.1 (1/s) and strain ranging from 0.1 to 10% used to determine the linear viscoelastic region (LVR). **b)** Frequency sweep performed at a constant strain of 0.25% (within the LVR since LVR clearly extends up to 1% strain) and strain rate ranging from 0.1 to 10 1/s used to determine both storage modulus G' (dark blue) and loss modulus G'' (cyan), **c)** Same frequency sweep performed to extract complex viscosity (green) and loss factor tan (δ) (yellow).

4.3 Results

4.3.1 Analysis of Cell-Free Collagen-Fibronectin Scaffolds Viscoelastic Properties

We first determined whether varied microstructure would modulate the dynamic shear moduli of the COL-FN scaffolds, in absence of cells. Figure 4.2 summarizes the storage (elastic) and loss (viscous) moduli extracted from oscillatory frequency sweeps performed at constant strain of 0.25% (within the LVR regime) and strain rate ranging from 0.1 to 10 1/s for all cell-free scaffolds. According to our data, denser scaffolds (Well E) exhibited significantly higher storage moduli (Fig. 4.2.a) and also higher loss moduli (Fig. 4.2.b) than sparse scaffolds (Well A). These results suggest that, when subjected to shear, (even though shear strain is relatively small (0.25%)) the microstructure of cell-free scaffolds has a profound effect on its shear response, as indicated by (i) the significantly increased stiffness measured on the dense scaffolds composed of short and thin fibres, and (ii) the similar trend observed for the dissipative (loss) component.

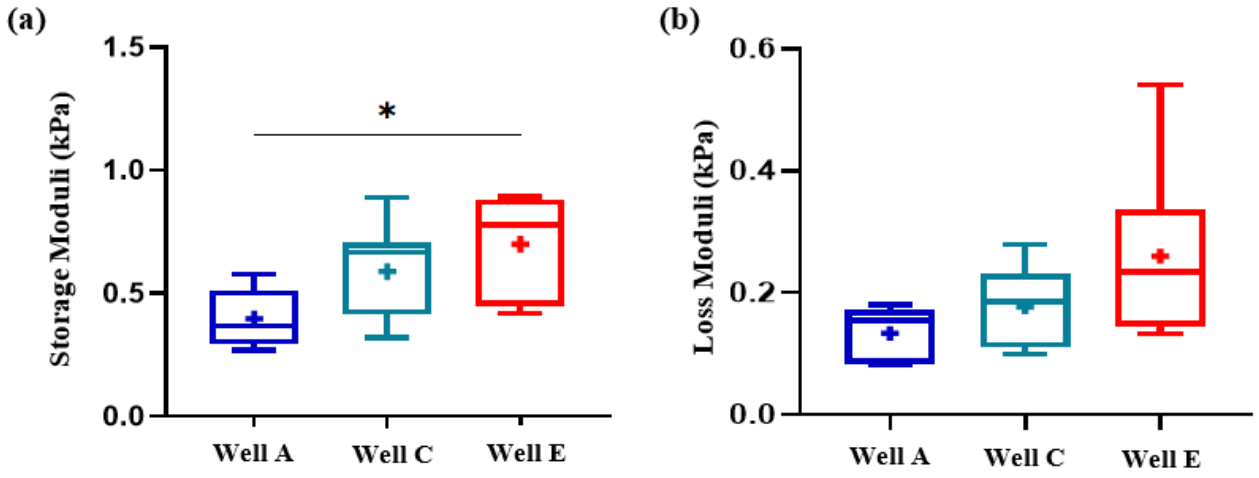

Figure 4.2 **Dynamic shear moduli of scaffolds with varied microstructure, in absence of cells (0.1 1/s, 0.25% strain)**. **a)** Averaged storage moduli, G' (Well A=0.397±0.122 kPa (n=5), Well C=0.589±0.206 (n=7), Well E=0.700±0.218 kPa (n=6)). **b)** Averaged loss moduli, G'' (Well A=0.133±0.047 kPa (n=5), Well C=0.177±0.070 (n=7), Well E=0.260±0.148 kPa (n =6)). (One-way ANOVA, *P < 0.05).

Since a clear trend was also observed in loss moduli, suggesting additional differences in the mechanical characteristics among the scaffolds, we next confirmed whether varied microstructure would also modulate the complex viscosity ($\eta*$), which corresponds to the overall resistance to flow (as a function of angular frequency (ω)). The complex viscosity is a frequency-dependent viscosity function, and it contains the dynamic in phase viscosity (η') or real part of

complex viscosity and the out of phase viscosity (η") or imaginary part of complex viscosity. Figure 4.3.a summarizes the complex viscosities ($\eta*$) extracted from oscillatory frequency sweeps performed at constant strain of 0.25% (within the LVR regime) and strain rate ranging from 0.1 to 10 1/s for all cell-free scaffolds. According to our data, high-density scaffolds (Well E) also exhibited significantly higher viscosities than low-density scaffolds (Well A), which validates the dissipative trend of loss moduli observed in Figure 4.2.b. These results suggest that, when subjected to small shear strains (0.25%), the microstructure of cell-free scaffolds has a significant effect on its viscous properties, as indicated by higher resistance, in other words, slower response to shear deformations (flow) for dense scaffolds composed of short and thin fibres.

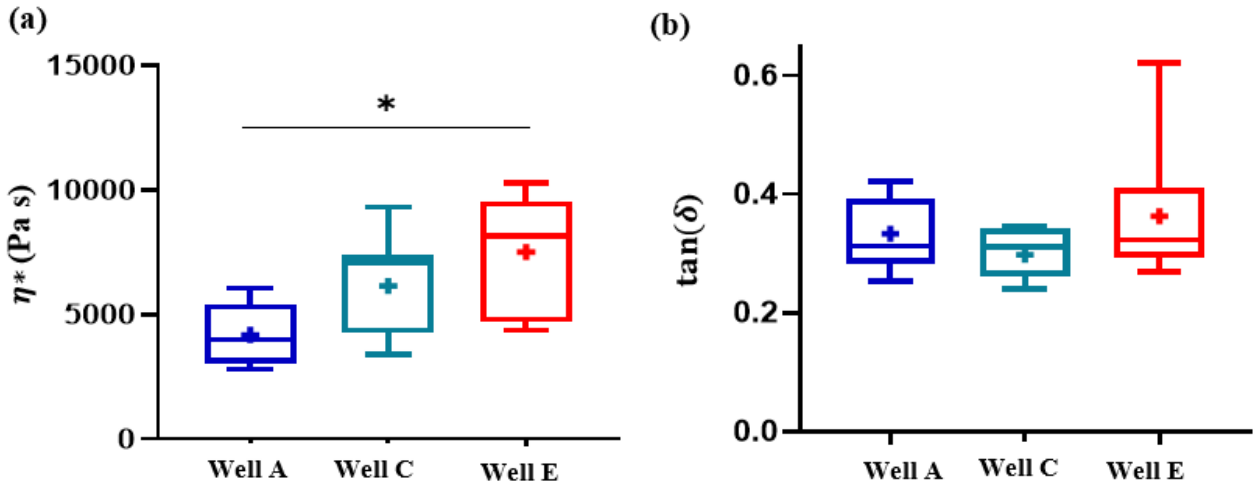

Figure 4.3 **Viscosity and loss factor of scaffolds with varied microstructure, in absence of cells (0.1 1/s, 0.25% strain)**. **a)** Averaged complex viscosity $\eta*$, (Well A=4190±1283 Pa s (n=5), Well C= 6156±2165 Pa s (n=7), Well E= 7518±2476 Pa s (n=6)). **b)** Averaged loss factor, tan(δ) (Well A= 0.333±0.063 (n=5), Well C= 0.298±0.041 (n=7), Well E= 0.363±0.129 (n=6)). (One-way ANOVA, *P < 0.05).

Importantly, to better describe the viscoelastic nature of our scaffolds, we also determined the relative contributions of the elastic and viscous components, by monitoring the loss factor, tan(δ) = G"/G', which determines the ratio between loss and storage moduli components of the dynamic shear moduli. Figure 4.3.b reports loss factors calculated at 0.1 1/s. Interestingly, no significant difference was observed among scaffolds. Instead, tan(δ) is nearly constant and significantly < 1 over the strain rate range investigated in this study, which suggests that, although viscoelastic by nature, all cell-free scaffolds possess a dominating elastic response.

4.3.2 Analysis of Cell-Loaded Collagen-Fibronectin Scaffolds Viscoelastic Properties

Next, we evaluated how varied microstructure would affect the dynamic shear moduli of all COL-FN scaffolds when they were loaded with cells. We repeated the amplitude sweeps needed to evaluate the LVR (data not shown), and we performed the frequency sweeps needed to extract both dynamic moduli. Figure 4.4 summarizes the storage (elastic) and loss (viscous) moduli extracted from oscillatory sweeps performed at constant strain of 0.25% (within the LVR regime) and strain rate ranging from 0.1 to 10 1/s for all cell-loaded scaffolds. Our data indicate no significant difference between storage moduli (Fig. 4.4.a) or loss moduli (Fig. 4.4.b) among cell-loaded scaffolds, regardless of their different microstructure (data not shown).[15] According to these results, despite an interesting trend observed in both storage and loss moduli suggesting that low-density cell-loaded scaffolds (Well A) may exhibit higher stiffness and viscosity than their high-density counterparts (Well C and Well E), the presence of cells seems to cancel out the effect of microstructure on viscoelastic properties.

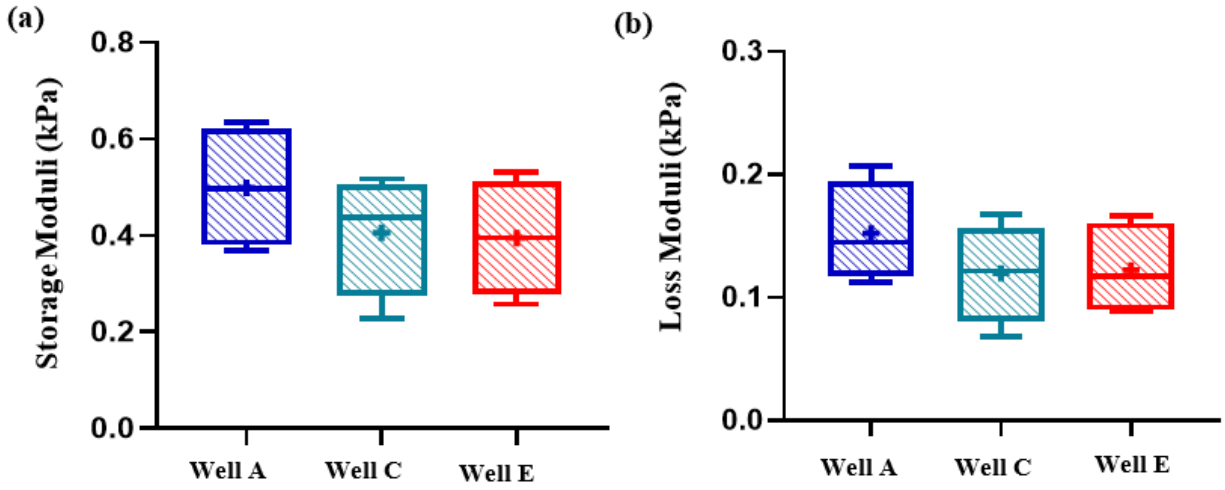

Figure 4.4 **Dynamic shear moduli of scaffolds with varied microstructure, in presence of cells (0.1 1/s, 0.25% strain)**. **a)** Averaged storage moduli, G′ (Well A=0.499±0.129 kPa (n=4), Well C=0.406±0.126 (n=4), Well E=0.395±0.122 kPa (n=4)). **b)** Averaged loss moduli, G″ (Well A=0.152±0.041 kPa (n=4), Well C=0.120±0.041 (n=4) and Well E=0.122±0.039 kPa (n=4)). (One-way ANOVA)

The same effect was found when we investigated cell-loaded scaffolds viscous properties (Figure 4.5.a), as no significant difference in complex viscosity ($\eta*$) was observed among scaffolds, regardless of their different microstructure, however, the trend shown is similar to that of loss modulus reported in Figure 4.4.b. Finally, we determined the loss factor $\tan(\delta)$ and, here

too, our results (Figure 4.5.b) indicate that it is (i) constant among scaffolds and (ii) significantly < 1 through the strain rate range investigated, which suggests that cell-loaded scaffolds also show a dominating elastic response in their overall viscoelastic behaviour.

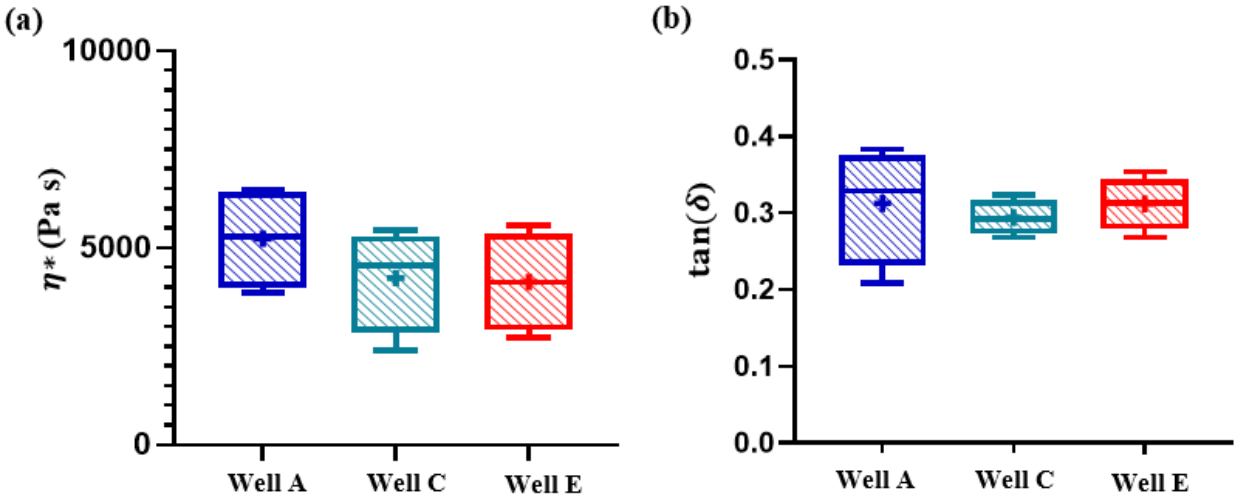

Figure 4.5 **Viscosity and loss factor of scaffolds with varied microstructure, in presence of cells (0.1 1/s, 0.25% strain)**. **a)** Averaged complex viscosity, $\eta*$ (Well A and E with the denser network. (Well A=5228±1300 Pa s (n=4), Well C= 4235±1321 Pa s (n=4), and Well E= 4135±1279 Pa s (n=4)). **b)** Averaged loss factor, tan(δ): (Well A= 0.313 ± 0.077 (n=4), Well C= 0.294±0.232 (n=4), and Well E= 0.312±0.035 (n=4)). (One-way ANOVA)

4.3.3 Effect of Strain on Cell-Free Scaffolds Viscoelastic Properties

While all trends shown above in Section 4.3.2 (cell-loaded scaffolds) were identical at both higher strains (0.5% and 1% strain) and higher strain rates (1 1/s and 10 1/s), the trends shown in Section 4.3.1 (cell-free scaffolds) exhibited a strain dependency, at all strain rates investigated, which we report here. Figure 4.6 summarizes storage moduli, loss moduli and complex viscosity extracted from oscillatory frequency sweeps performed at a constant strain of 1% and strain rate ranging from 0.1 to 10 1/s, for all cell-free scaffolds (only data obtained at 0.1 1/s are shown). According to our data, high-density scaffolds (Well E) exhibit significantly lower storage moduli and viscosities than low-density scaffolds (Well A and Well C), when they are subjected to higher shear strains. Interestingly, these results, obtained at 1% strain, are opposite to those seen in Section 4.3.1, obtained at 0.25% strain. This new trend suggests that strain levels have an apparent nonlinear effect on the mechanics of cell-free scaffolds, in particular, a clear strain softening when those are dense. Possible modes of shear-induced deformations of fibrillar scaffolds and the

relevance of shear strain values in physiological cell-mediated ECM remodelling are discussed in Section 4.4.

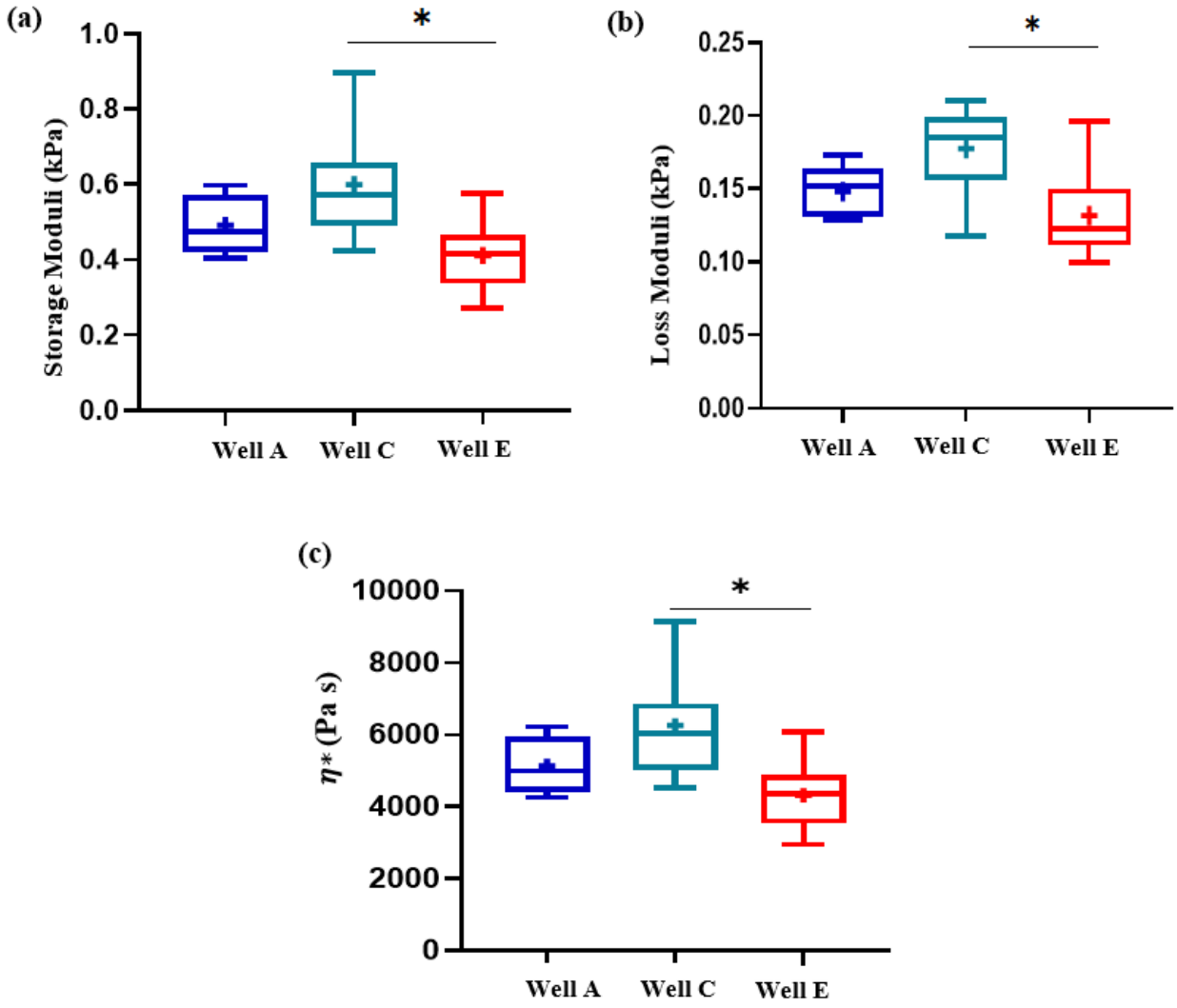

Figure 4.6 **Dynamic shear moduli and viscosity of cell-free scaffolds measured at higher shear strain (0.1 1/s, 1% strain)**. **a)** Averaged storage moduli, G' (Well A=0.4916±0.079kPa) (n=5), Well C =0.600±0.155) (n=7), Well E= 0.411±0.100kPa) (n=6). **b)** Averaged loss moduli, G″ (Well A=0.148±0.018 kPa (n=5), Well C=0.177±0.031 (n=7), Well E=0.132±0.033 kPa) (n=6). **c)** Averaged complex viscosities, $\eta*$ (Well A=5136±803.4 Pa s (n=5), Well C=6261±1546 Pa s) (n=7), Well E 4322±1032 Pa s) (n=6)). (One-way ANOVA) Mean ± SD. *P<0.05.

4.4 Discussion

In this study, our objective was to determine how the differently fabricated fibrillar COL-FN scaffolds differed in their rheological properties, and if those rheological differences depended on the presence of cells. Oscillatory frequency sweeps (G', G'') were performed in our parallel-plate rheometer, within the linear (LVR) regime, to characterize the viscoelastic properties of all scaffolds. The dynamic (storage and loss) moduli, complex viscosity and loss factor were determined via frequency sweeps performed at strains of 0.25%, 0.5%, and 1% over strain rates ranging from 10 to 0.1 1/s. All data shown are averages of a minimum of three independently prepared samples. In presence of cells, all viscoelastic trends were identical at all strains and all strain rates investigated, which is why we report only data obtained at 0.25% strain and 0.1 1/s. Instead, in absence of cells, viscoelastic trends exhibited a significant strain dependency, which is why we report data obtained at both 0.25% and 1% strain (keeping strain rate at 0.1 1/s).

In this section, we discuss both the effect of microstructure and the effect of cells' presence in the COL-FN scaffolds on their resulting viscoelastic properties. While in absence of cells, high-density scaffolds (Well E, warm-casted) exhibit higher stiffness and higher viscosity than low-density scaffolds (Well A, cold-casted), these microstructural-induced rheological differences vanish in presence of cells. Our results are consistent with other studies reporting that COL gels fabricated at high polymerization temperatures resulted in a denser and stiffer network when subjected to shear than those fabricated at low polymerization temperatures (the effect of cell contents was not reported).[17][18]

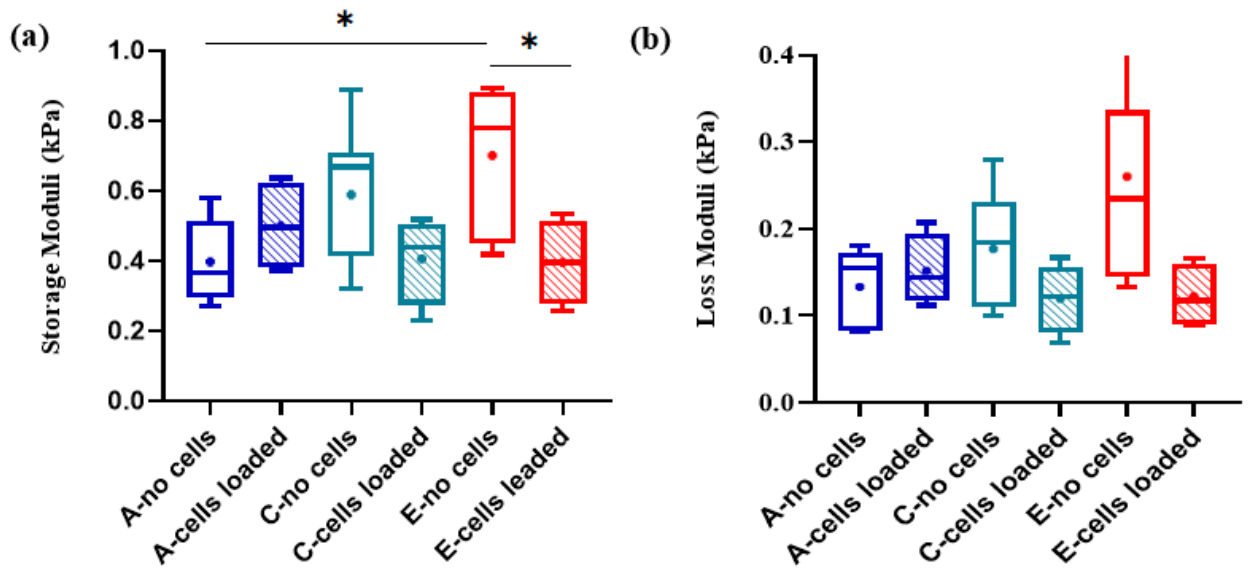

Figure 4.7 Comparison of dynamic shear moduli between cell-free and cell-loaded scaffolds (0.1 1/s, 0.25% strain). a) The storage moduli of scaffolds show that loading cells did not affect the elastic characteristics of scaffolds vastly except in well E which is lowered significantly. **b)** The loss moduli also show no significant differences between scaffolds with and without cells. (One-way ANOVA and unpaired t-test) Mean ± SD. *P<0.05.

To determine the effect of cells on viscoelastic trends, namely the effect of cells on the viscoelastic characteristics' dependency on scaffold microarchitecture, we have summarized our results in two additional figures. Figures 4.7 and 4.8.a display all dynamic shear moduli and complex viscosities obtained for cell-free and cell-loaded scaffolds at 0.25% strain and 0.1 1/s. While the presence of cells tended to increase both storage modulus and viscosity of low-density scaffolds (Well A), it had a clear opposite effect on the high-density scaffolds (Well C and Well E), indicated by a significant decrease of both storage modulus and complex viscosity. These results indicate that cells profoundly affect the shear-induced viscoelastic properties of scaffolds in different ways, highly depending on scaffold/matrix density, because they likely establish different types (and number) of cell-matrix interactions. First, cells might play different 'mechanical' roles by simply modifying the size of pores in the scaffolds (we have preliminary structural data showing that this happens in scaffolds after 48h of cell remodelling, data not shown). Briefly, in dense fibrillar networks such as Well E, cells might act as spacers between the tightly packed fibres, hence lower network density, which would in turn decrease overall stiffness and accelerate flow in response to shear. Instead, in a sparse fibrillar network such as Well A, cells

could localize within the initially large pores, tending to reduce pores' size, which would contribute to increasing overall network stiffness and viscosity. Second, more numerous cell-matrix interactions would also tend to thicken individual fibres and/or increase inter-fibres crosslinking, which could as well promote stiffening of initially low-density (large mesh size) networks and decelerate their overall flow in response to shear stresses.

To complete our investigation of scaffolds' viscoelastic properties, importantly, we also summarized the overall trend of the loss factor across all conditions (Figure 4.8.b). Our data reveal that the loss factor remained constant at ~ 0.3, regardless of scaffold microstructure and regardless of cell content, even though a trend (no significant difference) was noticeable, which may suggest a cell-induced decrease in $\tan(\delta)$, in denser scaffolds. Therefore, while the presence of cells impacts significantly scaffolds' rheological properties such as storage modulus and dissipation (viscosity), especially in dense networks, as previously reported [19][20], our results also suggest cells do not affect the ratio of loss versus storage moduli, indicating an overall predominant elastic response of all Col-FN scaffolds. (over a strain rate range of 0.1 to 10 1/s)

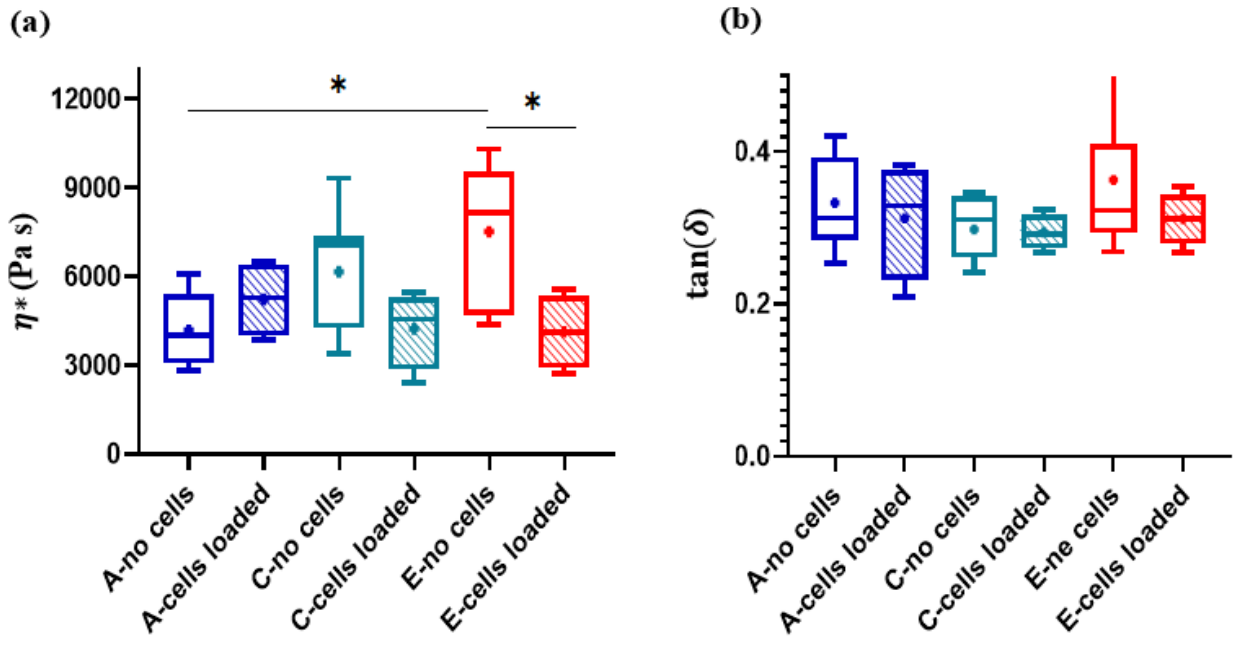

Figure 4.8 **Comparison of complex viscosity and loss factor between cell-free and cell-loaded scaffolds (0.1 1/s, 0.25% strain)**. **a)** The complex viscosity of gels shows that loading cells did not affect the viscous characteristics of scaffolds vastly except in well E which is lowered significantly. **b)** The loss factor for all scaffolds irrespective of the presence of cells shows a value below 1 representing the elastic dominating response. (One-way ANOVA and unpaired t-test) Mean ± SD. *P<0.05

The uncertainty seen in our rheological data arises from several factors among which most of them have been listed in the Discussion section of Chapter 3 already. Sample dehydration could have happened although we tried to keep hydration level constant through frequent DI pipetting during measurements. Slight variations in initial prestress were inevitable due to varied initial sample thickness of the hydrogels, however, variations in prestress values were much smaller in our rheological study than in our DMA study due to (i) overall higher thickness of samples used for rheology and (ii) more accurate initial plate alignment ensured by highly controlled parallelism between plates in the rheometer. Furthermore, one mechanism behind the viscoelastic response of fibrous hydrogels is shear-induced fibre lengthening, which would then modify initial shear conditions in gels subjected to consecutive oscillatory shear experiments (as was the case in our study). In fact, individual COL fibres are composed of several parallel fibrils, and, as reported in several studies, COL fibre lengthening under shear causes irreversible slippage between the fibrils, which dissipates energy and leads to mechanical relaxation.[21][9][22] Nevertheless, such shear-induced fibre lengthening is only expected at really large strains which is not the case here.

Finally, while all viscoelastic trends determined on cell-loaded scaffolds were identical at all strains (0.25 %, 0.5% and 1% strain) and all strain rates (0.1 1/s, 1 1/s and 10 1/s), interestingly, the trends determined on cell-free scaffolds revealed the same strain dependency at all strain rates (0.1 1/s, 1 1/s and 10 1/s). According to our data, while, as expected, high-density scaffolds (Well E) exhibit significantly higher stiffness and viscosity than low-density scaffolds (Well A) at very low strains (0.25%), they exhibit an opposite trend at higher strains (1%). In other words, when scaffolds are subjected to higher shear strains, dense scaffolds are more compliant and less viscous than their sparse counterparts (which could be explained by a shear softening due to network disruption of a more brittle scaffold). This trend is in agreement with data reported by Seo et al.[22] In their rheological analysis of cell-free COL gels performed at strains of 1–10 % (significantly larger strains than in our study), the authors reported increased shear moduli for gels with lower density composed of thicker and longer COL fibres. They attributed this unexpected effect to (i) increased thickness of individual fibres, leading to their increased stiffness, and to (ii) increased fibre buckling enabled by the larger distance between each collagen crosslink in low-density scaffolds with respect to high-density scaffolds (buckled fibres providing less resistance to the shear-induced realignment of stretched fibres, these low-density scaffolds can stiffen more

significantly under large strains). These mechanisms could explain the trends observed in our cell-free COL-FN networks, as our sparse (low-density, Well A) scaffolds are also composed of long and thick COL fibres, which may result in overall scaffold stiffening when subjected to high shear stresses.

Nonlinear elastic, viscoelastic and poroelastic behaviours have been seen in various biopolymer networks in response to changes in mechanical forces.[23] Van Oosten and coworkers report measurements and simulations of axial and shear stresses in collagen and fibrin hydrogels subjected to simultaneous uniaxial and shear strains (1–100%) at strain rates of 10 1/s and 1 1/s, in which they show that Young's moduli of the biopolymers' networks were not proportional to their shear moduli.[23] More specifically, nonlinear elasticity, in particular strain stiffening, was observed in COL networks [24] independently of polymerization conditions (i.e. temperature) and was attributed to an increase in local fibre alignment which was highly nonlinear [25][26] and a transition from filament bending to stretching.[27][28][29] According to the fibre network model, when COL gels are under shear stresses, strain stiffening is initiated, in which reorientation of originally randomly oriented fibres occurs to align them in strain direction, with fibre buckling along the direction of minimum stretch, however, such strain stiffening is expected only in a larger strain regime [25] Previous studies have also shown that dense COL networks exhibit variations in the onset of strain stiffening, with lower critical strains at which strain stiffening happens, resulting in overall decreased stiffness of the gels when subjected to higher strains.[30][31]

4.5 Conclusions

In this study, we investigated thoroughly the rheological properties of COL-FN networks subjected to oscillatory shear to better understand the relationship between microstructure, mechanics, and cell contents. Collectively, our data indicate that, in absence of cells, rheological properties were strain-dependent: while at low strains, high-density scaffolds exhibited significantly higher stiffness and viscosity than low-density scaffolds, the opposite trend was observed at higher strains. Our results also show that, in presence of cells, rheological trends did not depend either on strain or strain rate. The presence of cells was found to impact significantly scaffolds' rheological properties such as storage modulus and viscosity in high-density networks, however, it did not affect the loss factor, indicating a constant predominantly elastic response of

all COL-FN scaffolds, regardless of their microstructure and their cells' content (at least over strain rates ranging from 0.1 to 10 1/s).

In addition to significant progress in biomechanics and mechanobiology, recently, many studies have focused on tissue viscoelasticity. Our results suggest that the viscoelastic properties of COL-FN networks are sensitive to changes in the microarchitecture of the networks, achieved by varying the polymerization temperature. In conclusion, changing the polymerization temperature of hydrogels represents an easy and systematic way to tune network and individual fibre characteristics, which in turn, modify both the elastic and viscoelastic properties of the network, in a controlled manner. Although our findings in this study are promising, a more comprehensive rheological investigation is needed to develop a deeper knowledge of the structure-mechanics relationship of these materials. As such, this study provides a promising preliminary characteristic of materials for further investigations, and it provides a reliable platform for future cell-matrix and tissue engineering research studies.

4.6 References

1 Nelson CM, Bissell MJ. 2006. Of Extracellular Matrix, Scaffolds, and Signaling: Tissue Architecture Regulates Development, Homeostasis, and Cancer. Annu. Rev. Cell Dev. Biol. **22**(1): 287.

2 Ovijit Chaudhuri, Luo Gu, Darinka Klumpers, Max Darnell SA et al. 2016. Hydrogels with tunable stress relaxation regulate stem cell fate and activity. Nat. Mater. **15**(3): 10.

3 Kasza KE, Rowat AC, Liu J, Angelini TE, Brangwynne CP, Koenderink GH, Weitz DA. 2007. The cell as a material. Curr. Opin. Cell Biol. **19**(1): 101.

4 Chen LH, Ng SP, Yu W, Zhou J, Wan KWF. 2013. A study of breast motion using non-linear dynamic FE analysis. Ergonomics. **56**(5): 868.

5 Chaudhuri O et al. 2016. Hydrogels with tunable stress relaxation regulate stem cell fate and activity. Nat. Mater. **15**(3): 326.

6 Gong Z et al. 2018. Matching material and cellular timescales maximizes cell spreading on viscoelastic substrates. Proc. Natl. Acad. Sci. U. S. A. **115**(12): E2686.

7 Cameron AR, Frith JE, Cooper-White JJ. 2011. The influence of substrate creep on mesenchymal stem cell behaviour and phenotype. Biomaterials. **32**(26): 5979.

8 Chaudhuri O, Gu L, Darnell M, Klumpers D, Bencherif SA, Weaver JC, Huebsch N, Mooney DJ. 2015. Substrate stress relaxation regulates cell spreading. Nat. Commun. **6**: 1.

9 Nam S, Hu KH, Butte MJ, Chaudhuri O. 2016. Strain-enhanced stress relaxation impacts nonlinear elasticity in collagen gels. Proc. Natl. Acad. Sci. **113**(20): 5492.

10 Kim J, Feng J, Jones CAR, Mao X, Sander LM, Levine H, Sun B. 2017. Stress-induced plasticity of dynamic collagen networks. Nat. Commun. **8**(1).

11 Nagapudi K, Brinkman WT, Thomas BS, Park JO, Srinivasarao M, Wright E, Conticello VP, Chaikof EL. 2005. Viscoelastic and mechanical behavior of recombinant protein elastomers. Biomaterials. **26**(23): 4695.

12 Knapp DM, Barocas VH, Moon AG, Yoo K, Petzold LR, Tranquillo RT. 1997. Rheology of reconstituted type I collagen gel in confined compression. J. Rheol. (N. Y. N. Y). **41**(5): 971.

13 Forgacs G, Newman SA, Hinner B, Maier CW, Sackmann E. 2003. Assembly of collagen matrices as a phase transition revealed by structural and rheologic studies. Biophys. J. **84**(2 I): 1272.

14 Pedersen JA, Swartz MA. 2005. Mechanobiology in the third dimension. Ann. Biomed. Eng. **33**(11): 1469.

15 Asadishekari M. Design and Engineering of 3D Collagen-Fibronectin Scaffolds for Wound Healing and Cancer Research. MSc Thesis University of Ottawa 2018.

16 Picart C, Piau JM, Gaillard H, Carpentier P. 1998. Blood low shear rate rheometry: Influence of fibrinogen level and hematocrit on slip and migrational effects. Biorheology. **35**(4–5): 335.

17 Raub CB, Suresh V, Krasieva T, Lyubovitsky J, Mih JD, Putnam AJ, Tromberg BJ, George SC. 2007. Noninvasive assessment of collagen gel microstructure and mechanics using multiphoton microscopy. Biophys. J. **92**(6): 2212.

18 Raub CB, Unruh J, Suresh V, Krasieva T, Lindmo T, Gratton E, Tromberg BJ, George SC. 2008. Image correlation spectroscopy of multiphoton images correlates with collagen mechanical properties. Biophys. J. **94**(6): 2361.

19 Zhao Y, Li Y, Mao S, Sun W, Yao R. 2015. The influence of printing parameters on cell survival rate and printability in microextrusion-based 3D cell printing technology. Biofabrication. **7**(4).

20 Diamantides N, Dugopolski C, Blahut E, Kennedy S, Bonassar LJ. 2019. High density cell seeding affects the rheology and printability of collagen bioinks. Biofabrication. **11**(4): 45016.

21 Münster S, Jawerth LM, Leslie BA, Weitz JI, Fabry B, Weitz DA. 2013. Strain history dependence of the nonlinear stress response of fibrin and collagen networks. Proc. Natl. Acad. Sci. U. S. A. **110**(30): 12197.

22 Seo BR et al. 2020. Collagen microarchitecture mechanically controls myofibroblast differentiation. Proc. Natl. Acad. Sci. U. S. A. **117**(21).

23 Van Oosten ASG, Vahabi M, Licup AJ, Sharma A, Galie PA, MacKintosh FC, Janmey PA. 2016. Uncoupling shear and uniaxial elastic moduli of semiflexible biopolymer networks: Compression-softening and stretch-stiffening. Sci. Rep. **6**(December 2015): 1.

24 Storm C, Pastore JJ, MacKintosh FC, Lubensky TC, Janmey PA. 2005. Nonlinear elasticity in biological gels. Nature. **435**(7039): 191.

25 Licup AJ, Münster S, Sharma A, Sheinman M, Jawerth LM, Fabry B, Weitz DA, MacKintosh FC. 2015. Stress controls the mechanics of collagen networks. **112**(31).

26 Head DA, Levine AJ, MacKintosh FC. 2003. Distinct regimes of elastic response and deformation modes of cross-linked cytoskeletal and semiflexible polymer networks. Phys. Rev. E. Stat. Nonlin. Soft Matter Phys. **68**(6 Pt 1): 61907.

27 Abhilash AS, Baker BM, Trappmann B, Chen CS, Shenoy VB. 2014. Remodeling of fibrous extracellular matrices by contractile cells: Predictions from discrete fiber network simulations. Biophys. J. **107**(8): 1829.

28 Onck PR, Koeman T, Van Dillen T, Van Der Giessen E. 2005. Alternative explanation of stiffening in cross-linked semiflexible networks. Phys. Rev. Lett. **95**(17): 19.

29 Winer JP, Oake S, Janmey PA. 2009. Non-linear elasticity of extracellular matrices enables contractile cells to communicate local position and orientation. PLoS One. **4**(7).

30 Hall MS, Alisafaei F, Ban E, Feng X, Hui CY, Shenoy VB, Wu M. 2016. Fibrous nonlinear elasticity enables positive Mechanical feedback between cells and ECMs. Proc. Natl. Acad. Sci. U. S. A. **113**(49): 14043.

31 Abhilash AS, Baker BM, Trappmann B, Chen CS, Shenoy VB. 2014. Remodeling of fibrous extracellular matrices by contractile cells: Predictions from discrete fiber network simulations. Biophys. J. **107**(8): 1829.

Chapter 5: General Discussion, Conclusions and Future Directions

5.1 General Discussion

Fabrication of COL-FN Scaffolds with Varied Microstructure

Several studies have reported that both the structural and mechanical properties of ECM have a strong effect on cell morphology [1] and other key cellular functions such as proliferation, migration, differentiation.[2][3][4][5] To provide more insights into biological processes and tumour progression, it is essential to mimic properly the main features of the fibrillar ECM network by designing 3D scaffolds with tunable microstructure, mechanics and composition.[6] On one hand, fibrillar COL gels are composed of interconnected fibres/pores with overall structures that are highly sensitive to polymerization conditions. On the other hand, FN is the prominent glycoprotein of the ECM and can also form fibrillar structures in vitro, similar to COL.[7] It is also well established that, besides morphological features, ECM stiffness and overall density significantly impact cell response in both physiological and pathological (cancer) environments.[8][9][10] Studies have shown that increased density and stiffness of the breast tissue are correlated with breast cancer risk and aggression.[11][12][13][14] Because gels' mechanical properties are highly affected by their microstructure, tuning the overall structure and fibre topology of fibrillar networks is one of the fundamental objectives of (bio)materials science. Next, to fully characterize the mechanical properties of those hydrogels, different types of deformations including tension, compression, and shear are commonly used.[15]

The objective of this thesis was to assess all mechanical characteristics of ECM-mimetics relevant to their biological function, for use in mechanobiology (cancer) research and tissue engineering. More specifically, we focused on the evaluation of both purely elastic and viscoelastic properties of COL-FN fibrillar scaffolds, in absence or presence of highly aggressive breast cancer MDA-MB-231 cells, when subjected to compressive and shear stresses, respectively. First, we used a temperature-mediated casting method to fabricate three types of cell-free and cell-loaded 3D scaffolds, composed of both COL and FN fibres, with low, medium or high overall network density.[16] Next, scaffolds microstructure was determined via laser scanning confocal microscopy, revealing that warm-casted scaffolds exhibited a dense network composed of short and thin fibres, while cold-casted scaffolds showed sparse networks composed of long and thick

fibres. Scaffolds fabricated at intermediate casting temperatures displayed intermediate properties in terms of density and fibre topology, confirming that we could successfully generate a series of 3D ECM-mimicking scaffolds with gradual variations in microstructure, which properties would vary from those of the physiological (low-density) to the pathological (high density) cell microenvironment.

Compression Testing

In our first approach, we performed compression tests, using a custom-made Dynamic Mechanical Analyzer (DMA) to estimate Young's moduli of scaffolds in the presence and absence of cells at a velocity of 25 μm/s and maximum applied strain of 25%.

First, our DMA data obtained on cell-free scaffolds indicated that, despite a trend suggesting higher stiffness of high-density scaffolds with respect to their low-density counterparts, there was no significant difference in compressive elastic moduli among samples, regardless of their microstructure. Second, our results obtained on cell-loaded scaffolds suggest that the presence of cells might affect the mechanics of scaffolds in different ways, as cells tended to decrease the stiffness of high-density scaffolds while they tended to increase that of low-density scaffolds. However, again, this effect was not statistically significant.

In fact, all cell-free and cell-laden scaffolds exhibited a similar averaged Young's compressive modulus of ~ 2 kPa, which corresponds to the softer/compliant range of native tissues. In tissue engineering, the control of the compressive modulus of hydrogels is essential to ensure hydrogel biological functions. For instance, it was reported that neuronal cells survived longer in softer hydrogels with compressive moduli below 3.8 kPa than in stiffer hydrogels.[17]

To sum up, using the DMA technique we were not able to find any significant difference in stiffness between scaffolds, regardless of their microstructure and their cell contents. In fact, our macroscale compression tests failed to fully characterize scaffolds' mechanics and distinguish existing structural variations in the scaffolds. Our data are consistent with Seo et al. [18] who also showed that polymerization temperature of COL gels did not affect overall stiffness, as measured by DMA and/or AFM compressive testing. Collectively, these findings indicate that macroscale quasi-static compression testing may not the proper method to distinguish mechanical differences

in gels.[19][20] As such, an in-depth rheological investigation of these materials is required. In particular since, in the body, our tissues are subjected to complex shear forces in addition to simple tensile and compressive loads.

Rheology Testing

In our second approach, we performed comprehensive rheology measurements to explore whether the fabrication-dependent changes in microstructure modulate the viscoelastic properties of our scaffolds, in the presence and absence of cells. Through oscillatory shear measurements, the behaviour of hydrogels over both short and long-time scales could be readily assessed by measuring the dynamic shear moduli and viscosity of the materials, as a function of strain rate.

First, we performed oscillatory frequency sweeps at strain rates ranging from 0.1 to 10 1/s within the (previously determined) linear viscoelastic region (0.25%), i.e., in the region where storage (elastic) modulus G' and loss (dissipative/viscous) modulus G'' are independent of shear strain. Our data for cell-free scaffolds indicated that high-density scaffolds composed of short and thin fibres were both stiffer and more viscous than low-density scaffolds composed of long and thick fibres. Instead, our data for cell-loaded scaffolds indicated no significant dependency of viscoelastic properties on microstructure.

Next, we analyzed the effect of cells on gels of similar microstructure, and we observed that while the presence of MDA-MB-231 cells tended to increase both stiffness and viscosity of low-density scaffolds, it had a clear opposite effect on high-density scaffolds, indicated by a significant decrease of both storage modulus and complex viscosity. These results indicate that cells profoundly affect the shear-induced viscoelastic properties of scaffolds, but they do so in different ways, highly depending on scaffold/matrix density because they likely establish different types (and number) of cell-matrix interactions. These changes might be due to (i) cell-induced changes in the network pore size, increasing mesh size of sparse networks (filling up the holes) while decreasing mesh size of denser networks (acting as spacers between tightly packed fibres) or (ii) cell-induced thickening of individual fibres which would result in fibres' stiffening and/or (iii) cell-induced "crosslinking" effect on the network. Our latest microscopy imaging also indicates that cell-laden sparse networks (Well A) tended to exhibit inhomogeneous cell distribution (hence more prone to phase separation) than their denser counterpart (Well E).

Our loss factor data reveal that it remained constant at ~ 0.3, regardless of scaffold microstructure and cell content. Therefore, while the presence of cells impacts significantly scaffolds' rheological properties such as storage modulus and viscosity (especially in dense networks), it does not affect the ratio of loss versus storage moduli, indicating a constant predominantly elastic response of all COL-FN scaffolds (over a strain rate range of 0.1 to 10 1/s).

Finally, while all viscoelastic trends determined on cell-loaded scaffolds were identical at all strains (0.25 %, 0.5% and 1% strain) and all strain rates (0.1 1/s, 1 1/s and 10 1/s), interestingly, the trends determined on cell-free scaffolds revealed a strain dependency observable at all strain rates (0.1 1/s, 1 1/s and 10 1/s). According to our data, while, as expected, high-density scaffolds exhibited significantly higher stiffness and viscosity than low-density scaffolds at very low strains (0.25%), they exhibited an opposite trend at higher strains (1%). In other words, when scaffolds were subjected to higher shear strains, unexpectedly, high-density scaffolds were more compliant and less viscous than their low-density counterparts. According to the fibre network model, applying shear stresses to COL gels leads to reorientation/alignment of initially randomly oriented fibres in the stretching direction (strain stiffening is initiated).[21] Consequently, fibre-buckling is enhanced in more porous, low-density networks under shear, which provides less resistance to the realignment of stretched fibres, hence, upon increasing shear strain levels, low-density scaffolds stiffen more significantly than high-density scaffolds.

5.2 Conclusions

In the present study, we could generate three-dimensional ECM-mimicking COL-FN platforms with controlled structure and mechanics. We successfully fabricated both cell-free and cell-loaded COL-FN fibrillar scaffolds using temperature mediated casting, a technique that has been found to gradually tune the architecture of the networks.[16][22][23]

Our dynamic mechanical analysis in compression mode failed to determine significant differences in stiffness between scaffolds, indicating an average Young's modulus of circa 2 kPa for all scaffolds, regardless of their microstructure and/or cells' content. Instead, our comprehensive rheological analysis revealed important viscoelastic trends among which (i) high sensitivity of both viscous and elastic properties to scaffolds microstructure, including a strain dependency of both storage moduli and viscosity in cell-free scaffolds, (ii) a significant effect of

cell content on overall viscoelasticity (stiffness and viscosity), especially in high-density scaffolds, and (iii) an overall predominantly elastic response of all scaffolds, regardless of microstructure and cellular content.

Collectively, in this study, we could develop a library of compliant ECM-mimicking scaffolds made of interconnected COL and FN fibres, with specific and controlled structural along with mechanical properties, able to replicate either physiological (low density) or pathological (high density) cellular microenvironments. As such, these 3D tunable scaffolds represent valuable platforms for basic research (for example improving our understanding of the role of individual fibre architecture versus overall matrix morphology in cellular activity) but also for drug evaluation, and tissue engineering applications. Additionally, we could establish a correlation between the microstructure and the mechanics (elastic and viscoelastic properties) of the COL-FN fibrillar networks both in the absence and the presence of cells. Collectively, our findings also emphasize the need for such 3D environmental control for a better understanding of cancer mechanosignaling, particularly tumour growth and metastasis, and may help to expand knowledge of cell functions in large volumes within scaffolds of tunable microarchitectures.

5.3 Future Directions

Numerous studies have focused on controlling 3D matrix microarchitecture and mechanical properties by tuning the polymerization temperature of COL gels. The emphasis of this thesis was on the engineering and characterization of 3D ECM-mimicking biomaterials, in particular, on investigating their mechanical and rheological characteristics. COL-based hydrogels are commonly used to assess tumour cell behaviour as in vitro ECM models, in 3D microenvironments, with tunable biochemical and biophysical characteristics.[24] For future studies to restate more realistic *in vivo* microenvironments, we will need to (i) increase cell density (ii) increase the complexity of the composition by adding other ECM components such as laminin and fibrin known to be involved in cancer, (iii) make efforts to control protein conformation (since it directly affects cell-matrix interactions). In the context of cancer, our fabricated scaffolds would be valuable tools for cancer mechanobiology in highly controlled (hence reproducible) environmental conditions, in particular, to study cancer cell proliferation, altered cell-matrix interactions, the role of tumour microenvironment structure and mechanics on tumour growth and vascularization.

The tumour microenvironment is well known to be stiffer than healthy tissues.[25] In terms of ECM (biomechanical) properties, several studies have reported the impact of ECM stiffness, fibre alignment, and porosity on cell phenotype and invasive behaviour of cancer cells.[14][26] Fibrous ECM proteins show considerably higher local stiffness than that of the bulk matrix.[27] According to recent studies, when the microenvironment of cells is locally rearranged, it consequently modifies cell mechanosignaling [27] which results in altered local stiffness with varied consequences in healthy and tumorous tissues.[28]

Finally, in response to mechanical stresses or strains, viscoelastic materials exhibit long stress relaxations and/or creep behaviour. Therefore, besides investigation on both micro- and macro-scale short-term mechanical and viscoelastic characteristics, long-term behaviour of gels (such as stress relaxation or creep) should also be quantified, since it is now widely understood that hydrogel stress relaxation (or creep) also affect essential cell functions (e.g. cell spreading, differentiation and proliferation of mesenchymal stem cells).[29]

Although there is lots of room for improvement, our tunable platforms enable a better understanding of the critical link between ECM structure and mechanics, with the ultimate goal of controlling cellular functions. As such they already represent a valuable tool for biomaterials and biophysics research, with many potential applications.

5.4 References

1 Sun M et al. 2018. Effects of matrix stiffness on the morphology, adhesion, proliferation and osteogenic differentiation of mesenchymal stem cells. Int. J. Med. Sci. **15**(3): 257.

2 Lo CM, Wang HB, Dembo M, Wang YL. 2000. Cell movement is guided by the rigidity of the substrate. Biophys. J. **79**(1): 144.

3 Engler AJ, Sen S, Sweeney HL, Discher DE. 2006. Matrix elasticity directs stem cell lineage specification. Cell. **126**(4): 677.

4 Carey SP, Kraning-Rush CM, Williams RM, Reinhart-King CA. 2012. Biophysical control of invasive tumor cell behavior by extracellular matrix microarchitecture. Biomaterials. **33**(16): 4157.

5 Aurand ER, Lampe KJ, Bjugstad KB. 2012. Defining and designing polymers and hydrogels for neural tissue engineering. Neurosci. Res. **72**(3): 199.

6 Cox TR, Erler JT. 2011. Remodeling and homeostasis of the extracellular matrix: Implications for fibrotic diseases and cancer. Model. Mech. **4**(2): 165.

7 Mosher DF. 1993. Assembly of fibronectin into extracellular matrix. Curr. Opin. Struct. Biol. **3**(2): 214.

8 Guthold M, Liu W, Sparks EA, Jawerth LM, Peng L, Falvo M, Superfine R, Hantgan RR, Lord ST. 2007. A comparison of the mechanical and structural properties of fibrin fibers with other protein fibers. Cell Biochem. Biophys. **49**(3): 165.

9 Noriega SE, Hasanova GI, Schneider MJ, Larsen GF, Subramanian A. 2012. Effect of fiber diameter on the spreading, proliferation and differentiation of chondrocytes on electrospun chitosan matrices. Cells Tissues Organs. **195**(3): 207.

10 Murphy CM, Duffy GP, Schindeler A, O'Brien FJ. 2016. Effect of collagen-glycosaminoglycan scaffold pore size on matrix mineralization and cellular behavior in different cell types. J. Biomed. Mater. Res. - Part A. **104**(1): 291.

11 Sun X, Sandhu R, Figueroa JD, Gierach GL, Sherman ME, Troester MA. 2014. Benign breast tissue composition in breast cancer patients: association with risk factors, clinical variables, and gene expression. Cancer Epidemiol. biomarkers Prev. a Publ. Am. Assoc.

Cancer Res. cosponsored by Am. Soc. Prev. Oncol. **23**(12): 2810.

12 Discher DE, Janmey P, Wang YL. 2005. Tissue cells feel and respond to the stiffness of their substrate. Science (80). **310**(5751): 1139.

13 Yeung T et al. 2005. Effects of substrate stiffness on cell morphology, cytoskeletal structure, and adhesion. Cell Motil. Cytoskeleton. **60**(1): 24.

14 Provenzano PP, Inman DR, Eliceiri KW, Knittel JG, Yan L, Rueden CT, White JG, Keely PJ. 2008. Collagen density promotes mammary tumor initiation and progression. BMC Med. **6**: 1.

15 Antoine EE, Vlachos PP, Rylander MN. 2014. Review of collagen I hydrogels for bioengineered tissue microenvironments: Characterization of mechanics, structure, and transport. Tissue Eng. - Part B Rev. **20**(6): 683.

16 Asadishekari M. Design and Engineering of 3D Collagen-Fibronectin Scaffolds for Wound Healing and Cancer Research. MSc Thesis University of Ottawa 2018.

17 Lampe KJ, Mooney RG, Bjugstad KB, Mahoney MJ. 2010. Effect of macromer weight percent on neural cell growth in 2D and 3D nondegradable PEG hydrogel culture. J. Biomed. Mater. Res. - Part A. **94**(4): 1162.

18 Seo BR et al. 2020. Collagen microarchitecture mechanically controls myofibroblast differentiation. Proc. Natl. Acad. Sci. U. S. A. **117**(21).

19 Taufalele P V., VanderBurgh JA, Muñoz A, Zanotelli MR, Reinhart-King CA. 2019. Fiber alignment drives changes in architectural and mechanical features in collagen matrices. PLoS One. **14**(5): 1.

20 Xie J, Bao M, Bruekers SMC, Huck WTS. 2017. Collagen Gels with Different Fibrillar Microarchitectures Elicit Different Cellular Responses. ACS Appl. Mater. Interfaces. **9**(23): 19630.

21 Licup AJ, Münster S, Sharma A, Sheinman M, Jawerth LM, Fabry B, Weitz DA, MacKintosh FC. 2015. Stress controls the mechanics of collagen networks. **112**(31).

22 Staunton JR, Vieira W, Fung KL, Lake R, Devine A, Tanner K. 2016. Mechanical properties of the tumor stromal microenvironment probed in vitro and ex vivo by in situ-

calibrated optical trap-based active microrheology. Cell. Mol. Bioeng. **9**(3): 398.

23 Jansen KA, Licup AJ, Sharma A, Rens R, MacKintosh FC, Koenderink GH. 2018. The Role of Network Architecture in Collagen Mechanics. Biophys. J. **114**(11): 2665.

24 Wolf K, Alexander S, Schacht V, Coussens LM, von Andrian UH, van Rheenen J, Deryugina E, Friedl P. 2009. Collagen-based cell migration models in vitro and in vivo. Semin. Cell Dev. Biol. **20**(8): 931.

25 Freedman BR, Bade ND, Riggin CN, Zhang S, Haines PG, Ong KL, Janmey PA. 2015. The (dys)functional extracellular matrix. Biochim. Biophys. Acta - Mol. Cell Res. **1853**(11): 3153.

26 Provenzano PP, Eliceiri KW, Campbell JM, Inman DR, White JG, Keely PJ. 2006. Collagen reorganization at the tumor-stromal interface facilitates local invasion. BMC Med. **4**: 1.

27 Collet JP, Shuman H, Ledger RE, Lee S, Weisel JW. 2005. The elasticity of an individual fibrin fiber in a clot. Proc. Natl. Acad. Sci. U. S. A. **102**(26): 9133.

28 Acerbi I et al. 2015. Human breast cancer invasion and aggression correlates with ECM stiffening and immune cell infiltration. Integr. Biol. (United Kingdom). **7**(10): 1120.

29 Chaudhuri O. 2017. Viscoelastic hydrogels for 3D cell culture. Biomater. Sci. **5**(8): 1480.

Appendix

The dynamic moduli and complex viscosity were determined via frequency sweeps performed at strains of 0.5% and 1% at a strain rate of 0.1 1/s.

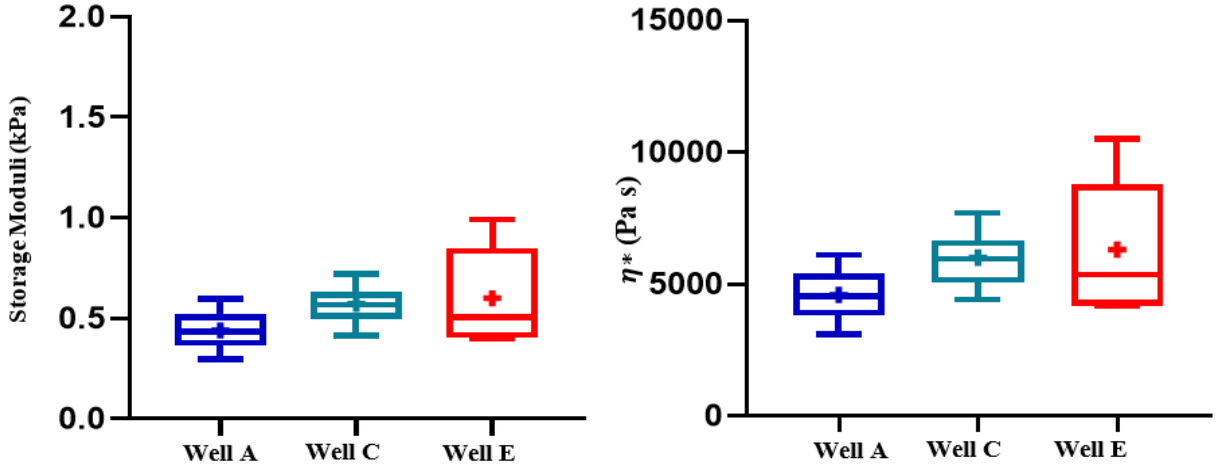

Figure A1 **Storage modulus and complex viscosity of scaffolds with varied microstructure in absence of cells (0.1 1/s, 0.5% strain). a)** Averaged storage moduli, G′ (Well A=0.441±0.106 kPa (n=5), Well C=0.572±0.0999 (n=7), Well E=0.601±0.243 kPa (n=6)). **b)** Averaged complex viscosity $\eta*$, (Well A=4588±1060 Pa s (n=5), Well C= 6011±1090 Pa s (n=7), Well E= 6302±2552 Pa s (n=6)).

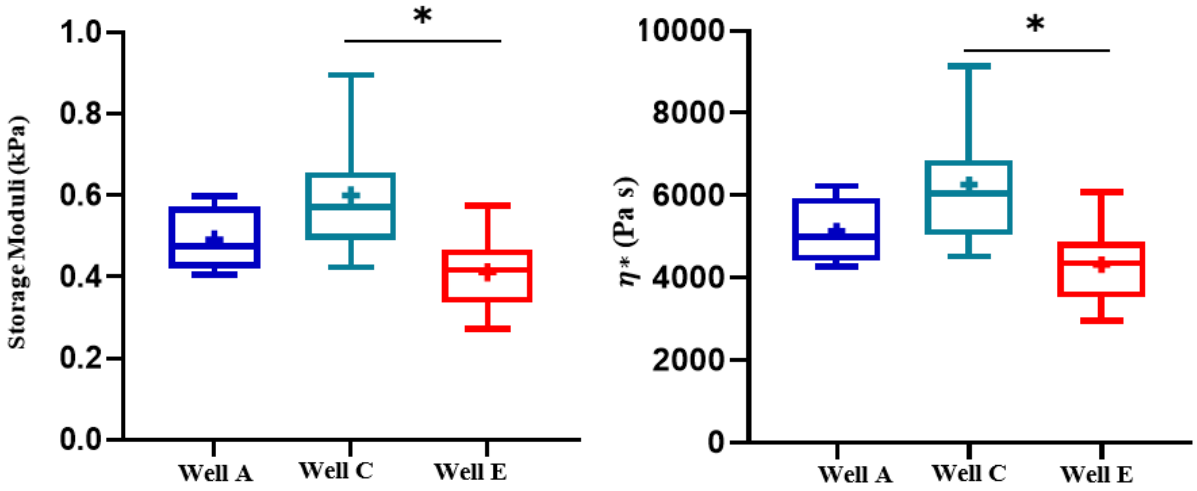

Figure A2 **Storage modulus and complex viscosity of scaffolds with varied microstructure in absence of cells (0.1 1/s, 1% strain). a)** Averaged storage moduli, G′ (Well A=0.492±0.079 kPa (n=5), Well C=0.599±0.155 (n=7), Well E=0.411±0.099 kPa (n=6)). **b)** Averaged complex viscosity $\eta*$, (Well A=5136±803.4 Pa s (n=5), Well C= 6261±1546 Pa s (n=7), Well E= 4322±1032 Pa s (n=6)).

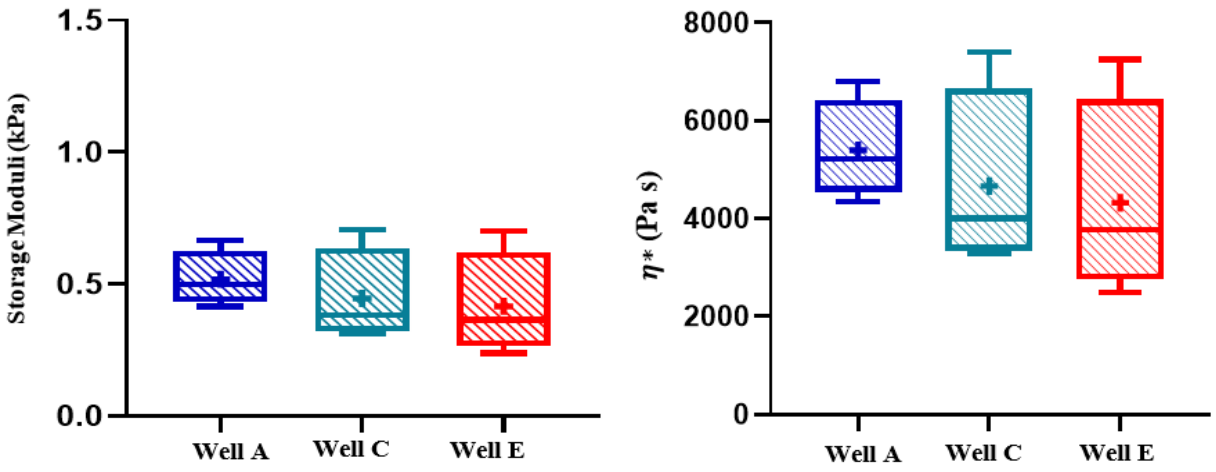

Figure A3 **Storage modulus and complex viscosity of scaffolds with varied microstructure, in presence of cells (0.1 1/s, 0.5% strain)**. **a)** Averaged storage moduli, G′ (Well A=0.518±0.106 kPa (n=4), Well C=0.446±0.181 (n=4), Well E=0.416±0.199 kPa (n=4)). **b)** Averaged complex viscosity, $\eta*$ Well A=5395±1021 Pa s (n=4), Well C= 4665±1885 Pa s (n=4), and Well E= 4320±2049 Pa s (n=4)).

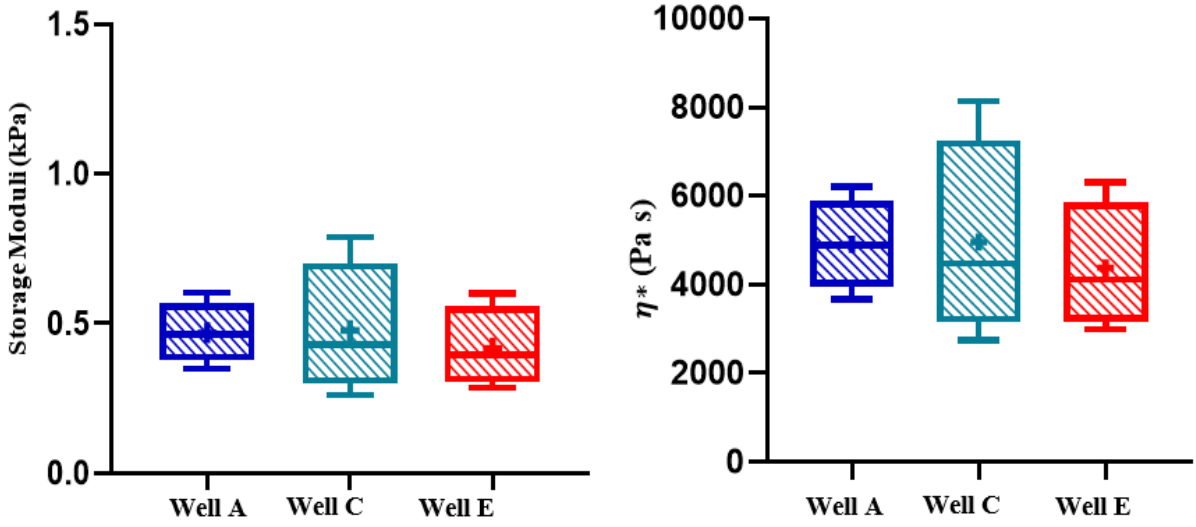

Figure A4 **Storage modulus and viscosity of scaffolds with varied microstructure, in presence of cells (0.1 1/s, 1% strain). a)** Averaged storage moduli, G′ (Well A=0.470±0.104 kPa (n=4), Well C=0.477±0.223 (n=4), Well E=0.419±0.135 kPa (n=4)). **b)** Averaged complex viscosity, $\eta*$ (Well A=4913±1037 Pa s (n=4), Well C=4960±2273 Pa s (n=4), and Well E=4378±1422 Pa s (n=4)).

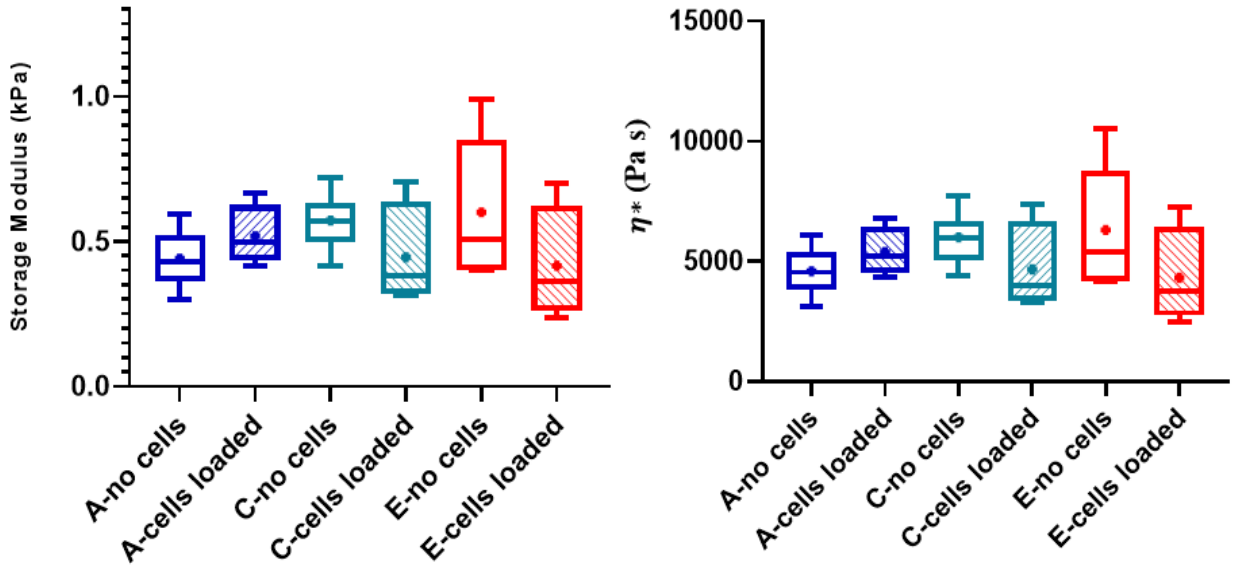

Figure A5 **Comparison of storage modulus and complex viscosity between cell-free and cell-loaded scaffolds (0.1 1/s, 0.5% strain). a)** The storage moduli of scaffolds show that loading cells did not affect the elastic characteristics of scaffolds vastly. **b)** The complex viscosity of gels shows that loading cells did not affect the viscous characteristics of scaffolds significantly.

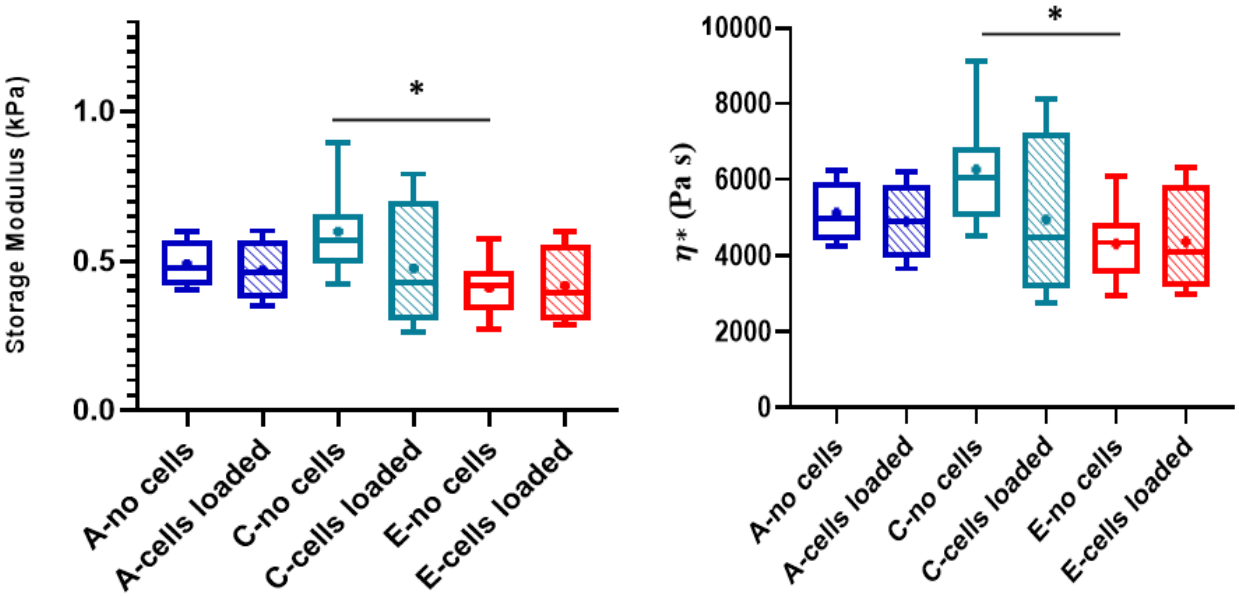

Figure A6 **Comparison of storage modulus and complex viscosity between cell-free and cell-loaded scaffolds (0.1 1/s, 1% strain). a)** The storage moduli of scaffolds show that loading cells did not affect the elastic characteristics of scaffolds significantly. **b)** The complex viscosity of gels shows that loading cells did not affect the viscous characteristics of scaffolds vastly.